nature communications

Article

https://doi.org/10.1038/s41467-026-72032-4

Highly mutagenic copying of telomeric circles promotes ALT establishment

Received: 3 August 2025

Accepted: 24 March 2026

Published online: 22 April 2026

Check for updates

Meng-Chia Tsai[1,5], Jacob M. Wells[1,5], Kelley A. Renninger[1], Kendra Musmaker[2], Ryan Pellow[2], Andrey Malkov[1], Josep M. Comeron[2,3] & Anna Malkova[1,4]

Alternative lengthening of telomeres (ALT) is a recombination-based pathway enabling cancer cells to maintain telomeres. ALT establishment remains poorly understood due to difficulties identifying its molecular steps. Here, using Oxford Nanopore sequencing and computational modeling, we track the evolution of individual chromosome end structures during ALT establishment in yeast and delineate three molecular milestones. First, homologous recombination via break-induced replication (BIR) at telomeres and sub-telomeric regions delays senescence. Second, BIR interruption and microhomology-mediated recombination promote initial telomere extension and telomeric circle formation. Third, the final extension—critical for chromosome end stabilization—utilizes a highly mutagenic replication mechanism to copy telomeric circles. Linking these newly defined ALT milestones is Mph1, the homolog of human FANCM, which plays important roles throughout ALT establishment by disrupting BIR synthesis and promoting template switching. Our findings support a model where template switching during DNA repair synthesis drives the transitioning through the multiple steps involved in ALT establishment and progression, ultimately producing ALT survivors.

Telomeres serve as protective caps on chromosome ends that aid in maintaining genome integrity and genetic stability. In the absence of telomerase, telomeres shorten with every round of DNA replication until a minimum length threshold is reached, which typically triggers cellular senescence[1–5]. Alternative lengthening of telomeres (ALT) is a mechanism for maintaining telomere length in telomerase-deficient cells using inter-telomere homologous recombination (HR)[6–8]. Notably, ALT is responsible for telomere maintenance in ~10–15% of human cancers[9–11] and is often activated in telomerase-proficient cancers after treatment with anti-telomerase drugs[12], making it critical to understand the mechanisms underlying ALT activation and establishment. However, although mammalian cancer cell models can probe telomere maintenance during ALT, it remains challenging to dissect the multi-step process of ALT establishment at the molecular level in these models. Meanwhile, yeast *Saccharomyces cerevisiae* has been used as a robust model to shed light on the ALT mechanism in eukaryotes, including humans. Inactivation of telomerase in yeast is sufficient to induce ALT, thus allowing molecular and genomic dynamics to be followed from the beginning of telomere shortening all the way through the formation of survivors that have successfully stabilized their chromosome ends using ALT (hereafter, "ALT survivors")[2,8,13,14].

Initial insights into the mechanisms underlying ALT came from Southern blot analysis of ALT survivors in yeast, which uncovered two distinct survivor types: Type I and Type II[13–16]. Type I survivors are thought to maintain their chromosome ends by forming tandem repeats of sub-telomeric Y′ elements adjacent to short terminal telomeric sequences, and these Type I survivors are characterized by a fluctuating rate of cellular division and unstable chromosome end structure[13]. In contrast, Type II survivors stabilize chromosome ends by

[1]Department of Biochemistry and Structural Biology, University of Texas Health Science Center at San Antonio, San Antonio, TX, USA. [2]Department of Biology, University of Iowa, Iowa City, IA, USA. [3]Interdisciplinary Graduate Program in Genetics, University of Iowa, Iowa City, IA, USA. [4]Greehey Children's Cancer Research Institute, University of Texas Health Science Center at San Antonio, San Antonio, TX, USA. [5]These authors contributed equally: Meng-Chia Tsai, Jacob M. Wells. e-mail: josep-comeron@uiowa.edu; malkova@uthscsa.edu

creating only long telomeric repeats and display a consistent growth rate comparable to a telomerase-positive population[13,15,16].

Genetic analyses initially suggested that the two types of ALT survivors are formed through two independent pathways, both of which employ break-induced replication (BIR). Specifically, it was observed that deleting either of the two main BIR genes, *RAD52* or *POL32*, eliminated both Type I and Type II ALT survivors[13,15,17], whereas the HR genes *RAD51*, *RAD54*, *RAD55*, and *RAD57* were required only for Type I survivors, while the HR genes *RAD59*, *RAD50*, and *SGS1* were required only for Type II survivors[14,16,18–20]. However, our recent study measuring the precise frequency of ALT survivor formation discovered that Rad51 and Rad59 contribute to both ALT survivor pathways, suggesting the mechanisms yielding ALT survivors are likely intertwined in a single, unified pathway[21].

Identification of the molecular milestones during ALT initiation, although crucial for understanding how survivors emerge, has been hindered by the low frequency and stochasticity of survivor formation, as well as the inability to delineate the structure of individual chromosome ends leading to ALT survivors. Lineage tracing studies on single cells have suggested the existence of early ALT precursors[22,23], but technical limitations have prevented longitudinal tracking of chromosome end structures to link these intermediates with resulting ALT survivors. Studies of chromosome end structures during ALT using Sanger sequencing detected the early extension of telomeric sequences and acquisition of Y' elements[24–26], but the observations were limited to only one (or a few) chromosome ends.

Here, we combined Oxford Nanopore Technologies (ONT) sequencing and computational modeling to identify the molecular steps of ALT establishment by longitudinally following telomere and sub-telomeric structures from the time of conditional telomerase inactivation through the formation of ALT survivors. Unlike human telomere repeats $(TTAGGG)_n$, the yeast telomere sequence is degenerate $(TG_{1\text{-}3})_n$, and this heterogeneity along yeast telomeres was exploited here to identify specific features of DNA recombination and synthesis at individual chromosome ends during ALT establishment. Using ONT sequencing, we identified the molecular milestones of ALT establishment, including (i) HR via BIR at telomeres and sub-telomeric regions, which delays cellular senescence; (ii) interruption of BIR and recombination at microhomologies, which promotes the initial telomere extension; and (iii) the generation and copying of telomeric circles (t-circles), which promotes the final telomere extension and stabilizes ALT survivors. We observed chromosome end characteristics that support a critical role for template switching early during ALT establishment as well as later during t-circle formation and copying. Finally, we report that Mph1 (the homolog of human FANCM) plays an important role during several steps of ALT establishment, supporting a model wherein Mph1 interrupts BIR synthesis and facilitates template switching to promote the establishment of ALT.

Results

Tracking ALT establishment in a telomerase shut-off system

Formation of ALT survivors has been historically studied in "telomerase-elimination" yeast strains lacking key telomerase subunits, such as TLC1 or Est2. In these strains, more than 25 population doublings (PDs) were required following tetrad dissection to form colonies, allowing only the later steps of ALT establishment to be followed[21]. To characterize events throughout ALT, from telomere erosion through ALT survivor formation, we adopted a telomerase shut-off experimental system in which the expression of *TLC1*, which encodes the RNA template subunit of telomerase, is inactivated by doxycycline.

This telomerase shut-off system was previously used to follow telomere dynamics after the onset of telomere erosion[22]; however, because telomerase inactivation in this system was incomplete, later ALT steps and survivors could not be characterized. This conclusion is supported by the observation that cell division in this system was never fully arrested (Supplementary Fig. 1a), consistent with previous reports[22,23,27–29]. In addition, RT–qPCR analysis showed that, although *TLC1* transcripts were significantly reduced 4 and 8 days after doxycycline addition, they remained at ~3–20% of initial levels (Supplementary Fig. 1b).

We overcame the limitation of incomplete telomerase suppression in the original shut-off system by also targeting Est2, the catalytic telomerase subunit, using an auxin-inducible degron (AID). In this new telomerase shut-off system (hereinafter WT; Fig. 1a), serial passaging at low cell density progressively reduced cell replicative capacity, eventually leading to ALT survivor formation in only ~5–10% of cultures (Fig. 1b). Using the Poisson distribution[21], we determined the frequency of ALT survivors in the new system to be 2×10^{-5} (Fig. 1b, c and Supplementary Fig. 1c), which is similar to the frequency in our telomerase-elimination system[21] (Fig. 1c (WT); compare to Supplementary Fig. 1d (*tlc1Δ*)). As predicted, in the new shut-off system, no ALT survivors were detected in the absence of Rad52, while *rad51Δ* and *rad59Δ* cells had significantly reduced (7-10x) ALT frequency (Fig. 1c and Supplementary Fig. 1d). Determining the number of Y' elements in ALT survivors by droplet digital PCR (ddPCR) showed that WT and *rad59Δ* cells had a mix of Type I and Type II ALT survivors, whereas only Type II survivors were observed in *rad51Δ* cells (Supplementary Fig. 1e), similar to results obtained in the telomerase-elimination system[21].

Next, we used our new system to test hypotheses regarding the genetic requirements of ALT establishment. Our recently proposed unified ALT pathway predicted that the annealing activity of Rad52 is involved in producing all ALT survivors[21]. We tested this in our telomerase shut-off system by introducing the *rad52-R70A* mutation, which disrupts the annealing activity of Rad52 without interfering with its ability to recruit Rad51[30] (Supplementary Fig. 2a), and we predicted that these cells should display a more severe ALT reduction phenotype than *rad51Δ* and *rad59Δ*. Indeed, a 40-fold decrease in ALT frequency was observed in *rad52-R70A* cells (5.1×10^{-7}), which was significantly lower compared with *rad51Δ* or *rad59Δ* (Fig. 1c and Supplementary Data 1). Like *rad59Δ* cells, both Type I and Type II ALT survivors were formed in *rad52-R70A* (Supplementary Fig. 1e).

Next, we deleted the translocase *RAD54* (Supplementary Fig. 2a), which resulted in an ALT frequency 44-fold lower (4.7×10^{-7}) than WT and also lower than the frequencies observed in *rad51Δ* or *rad59Δ* (Fig. 1c and Supplementary Data 1). A similar effect of *rad54Δ* on ALT survivors was observed in the telomerase-elimination system (Supplementary Fig. 1d). This ALT defect in *rad54Δ* cells may be similar to *rad54Δ*'s effect on BIR induced by a site-specific DNA break, where it impairs both Rad51-dependent and Rad51-independent BIR[31,32]. Together, the impacts of *rad52-R70A* and *rad54Δ* on all ALT survivors further support the unified ALT model.

Pif1 helicase is essential for BIR[33] and has been implicated in ALT[34]. We tested the effects of *pif1-m2* and *pif1-NLSΔ* mutants, which are specifically defective for Pif1 nuclear activities but not for mitochondrial functions[35,36], in the new telomerase shut-off system. As expected, ALT frequencies in both *pif1-m2* and *pif1-NLSΔ* cells were significantly decreased three-to-four-fold compared to WT cells (Fig. 1c and Supplementary Data 1). Interestingly, most ALT survivors in *pif1-NLSΔ* mutants had few copies of Y' elements and resembled Type II survivors (Supplementary Fig. 1e). It is possible that the intermediate phenotype of these *pif1* mutants stemmed from their previously described residual Pif1 nuclear activity[35–37], or it could be due to the longer starting telomere lengths in these mutants[36]. We also observed that, in the new system, the frequency of ALT survivors was increased 18-fold in the telomere-capping-deficient *rif1Δrif2Δ* mutant (Fig. 1c), consistent with our prior finding in the telomerase-elimination system[21].

Finally, we tested the role of another helicase, Mph1, which interrupts BIR by unwinding D-loops[38–44]. We observed a 2-fold increase in ALT survivor formation in *mph1Δ* compared with WT cells in the telomerase shut-off system and an 8-fold increase in the

https://doi.org/10.1038/s41467-026-72032-4

telomerase-elimination system (Fig. 1c, Supplementary Fig. 1d, and Supplementary Data 1).

Telomere dynamics during ALT establishment

To determine how ALT is established after telomerase inactivation, we longitudinally tracked individual chromosome end structures using ONT sequencing. In brief, we inactivated telomerase at population doubling (PD) 0 by simultaneous addition of IAA (auxin) and doxycycline, grew the culture for 24 hours, and took a sample for ONT sequencing as well as an aliquot (100 cells/mL) to inoculate a fresh culture containing auxin and doxycycline for the next time point.

To characterize telomere lengths at each chromosome end at each time point, two independent approaches were used to ensure that the analysis included only ONT reads that reached the end of the

Fig. 1 | Telomerase shut-off system enables telomere dynamics to be tracked from telomerase inactivation through formation of ALT survivors. a Overview of the telomerase shut-off strain (AM6991). Top: Diagram of shut-off system. Left: Tet-Off *TLC1* system where inactivation of *TLC1* is achieved by addition of doxycycline (yellow circles); Right: induced degradation of Est2 by auxin (red stars). Bottom: chromosome end structure of the AM6991 determined by ONT sequencing. Rectangles: Y′ elements (colors correspond to differentiable Y′ sequences). **b** Strategy for measuring ALT frequency by obtaining rare, independent ALT survivors. Top: cell passaging scheme (100 cells/mL were transferred at every passage). Bottom: survivorship curves of independent cultures. Only rarely do cultures produce ALT survivors, assuring their independence. Dashed line: cell number/mL passaged each day. Source data are provided as a Source Data file. **c** Effect of deletion of BIR and telomere maintenance genes on ALT frequency. Medians and 95% confidence intervals (in parentheses) of ALT frequencies are shown. Arrows and fold changes in ALT frequency are relative to WT (see Supplementary Data 1 for details). **d** Identifying telomere reads using the TeloTracker pipeline. Only reads anchoring to a single chromosome end with an ONT adapter flanking the telomere sequence at the read's end are classified as telomere reads. TeloTracker assigns reads to individual chromosome ends using chromosome-end-specific 5-kb "anchor" sequences, verifies the presence of ONT adapter sequences on the telomere ends of the reads, and annotates telomere lengths and other chromosome end features (see Methods for details). **e** Longitudinal analysis of telomere lengths by ONT sequencing. Telomere lengths of WT (AM6991) cell populations following telomerase inactivation. Representative data from one of two biological repeats are shown. Y-axis: the frequency of corresponding telomere lengths for each PD. Dotted lines: median telomere lengths. See Supplementary Fig. 3a, b, for details and additional repeats. A one-sided Mann-Whitney U test comparing telomere lengths shows significantly longer telomeres at an initial extension phase (PD 33 $n = 1580$ vs. PD 37 $n = 839$; $p = 3.07 \times 10^{-26}$) and a final extension phase (PD 37 $n = 839$ vs PD 44 $n = 1117$; $p < 2.23 \times 10^{-308}$); see Supplemental Data 2 and Methods for details. **a** Created in BioRender. Withers, K. (2026) https://BioRender.com/s12qa1l top panel of (**b**) created in BioRender. Withers, K. (2026) https://BioRender.com/4xr6zia and (**d**) created in BioRender. Withers, K. (2026) https://BioRender.com/qg9tu2i.

telomeres. The first approach used the established TeloTag protocol[45], wherein chromosome ends were tagged by special oligonucleotides, and only reads with both the special oligonucleotides and ONT adapters were considered to represent full-length telomere reads. The second approach employed our newly developed TeloTracker, which uses the ONT adapters themselves as indicators of sequencing reads that reach telomere ends, rather than relying on telomere-end-specific tagging (Fig. 1d and Supplementary Fig. 2b, c). We determined that these two methods produced similar telomere length distributions at all PDs (Supplementary Fig. 2c, d), but the TeloTag protocol yielded significantly fewer usable telomere reads for analysis and required a specific 3′-overhang telomere end structure, which could change during ALT establishment[46]. Therefore, we selected the TeloTracker methodology for subsequent analyses (Fig. 1d and Supplementary Fig. 2b, c).

As expected, prior to telomerase inactivation (PD 0), the distribution of telomere lengths in the telomerase shut-off system was symmetric, with a median telomere length of 158 bp (Fig. 1e and Supplementary Fig. 3a). After telomerase inactivation, the distribution of telomere lengths became skewed as telomeres were continuously shortened, reaching a minimum median length of 120 bp at PD 33 (Fig. 1e and Supplementary Fig. 3a). After the next passage (PD 37), median telomere length increased to 131 bp, indicative of a fraction of telomeres undergoing moderate initial telomere extension (Fig. 1e, Supplementary Fig. 3a, and Supplementary Data 2; see Methods for the details). Another increase in median telomere length was detected at PD 44, when many telomeres exceeded 1000 bp and the median length reached 518 bp, indicating a final telomere extension event (Fig. 1e and Supplementary Fig. 3a). Similar telomere dynamics were observed when we repeated this experiment (Supplementary Fig. 3b). Interestingly, while median telomere length changed continuously between PD 0 and PD 37, the 10th percentile reached its lowest level by PD 19 and remained relatively stable between 66-80 bp until PD 37 (Fig. 1e and Supplementary Fig. 3a, b). This stable 10th percentile of telomere length likely reflects a threshold at which telomeres become critically short and trigger cell cycle arrest and senescence, consistent with previous findings[21]. Importantly, similar telomere dynamics were observed in our telomerase-elimination system (Supplementary Fig. 4a).

Next, we evaluated telomere dynamics in ALT-defective *rad52Δ* and *rad54Δ* single mutants. In both strains, telomere dynamics were similar to early WT dynamics after telomerase shut-off (Fig. 2a, b and Supplementary Fig. 5a–e). However, unlike WT cells, neither mutant population was able to extend the eroded telomeres at any point. Similar telomere dynamics were observed in *rad51Δ* cultures (Fig. 2c and Supplementary Fig. 5f, g). In single-strand annealing (SSA)-defective *rad59Δ* and *rad52-R70A* mutants, cells underwent initial telomere extensions by PD 44, after reaching a minimum median length at PD 37 of 115–116 bp in *rad59Δ* (Fig. 2d and Supplementary Fig. 6a, b) and 117–120 bp in *rad52-R70A* (Fig. 2e and Supplementary Fig. 6c, d). Compared with WT, this initial telomere extension was significantly delayed, and no final extension was observed.

In the absence of Mph1, telomere erosion kinetics were similar to those observed in WT cells following telomerase shut off, but no telomere extension was observed through PD 44 (Fig. 2f and Supplementary Fig. 3c, d). When we extended our time course to PD 83, we observed only rare long telomeres (~ 2.5% of sequenced telomeres) in *mph1Δ* (Supplementary Fig. 7a), suggesting that both steps of extension occur only rarely in the absence of Mph1 (Fig. 2g, h).

Mph1 deletion promotes expansion of Y′ repeats

To reconcile the defective telomere extension with the high frequency of ALT that we observed in the absence of Mph1, we hypothesized that sub-telomeric regions may play a role in ALT dynamics. If so, we posited that *mph1Δ* cells may survive because they have more efficient HR at sub-telomeric regions, leading to expansion of Y′ tandem repeats. To test this, we obtained independent ALT survivors from both WT and *mph1Δ* liquid cultures (Fig. 3a). Analysis of Y′ elements using ddPCR showed that all (21/21) of the independent *mph1Δ* survivors possessed ≥198 Y′ elements each (Fig. 3b), a drastic increase compared to 34 Y′ elements in the reference genome (Fig. 1a). In contrast, only 2/21 WT survivors were characterized by a high number of Y′ elements (Fig. 3b). Further ONT sequencing analyses showed that, in the absence of Mph1, the chromosome ends consisted of short telomeres with greatly varying numbers of Y′ elements, comprising a heterogeneous, unstable population similar to what was previously described as Type I survivors[13] (hereafter referred to as "unstable" survivors) (Fig. 3c, d and Supplementary Fig. 7b, c). Meanwhile, most WT survivors had chromosome ends in which the number of Y′ elements were similar to the parental strain and adjoined to long telomeres, representing stable Type II survivors[13–16,21] (hereafter referred to as "stable" survivors) (Fig. 3e, f and Supplementary Fig. 7d). These data suggest that the formation of stable ALT survivors in WT cells involves a mechanism(s) that is defective in the absence of Mph1.

To understand how cells acquire Y′ elements during ALT establishment and the potential role of Mph1, we analyzed the number of Y′ elements in individual ONT sequencing reads obtained in the time course experiments described above (Figs. 1e, 2a–f, and Supplementary Figs. 3, 5, 6). As expected, no significant Y′ element gains were observed at any time point in *rad52Δ*, *rad51Δ*, or *rad54Δ* strains (Supplementary Fig. 7e–g). However, at PD 28-33, the number of reads showing gains in Y′ elements was similar in WT (3.16%) and *mph1Δ* (3.01%) (Supplementary Fig. 7h, i, 8a, b, and Supplementary Data 3). Interestingly, *mph1Δ* cells had significantly more gains of ≥2 Y′

https://doi.org/10.1038/s41467-026-72032-4

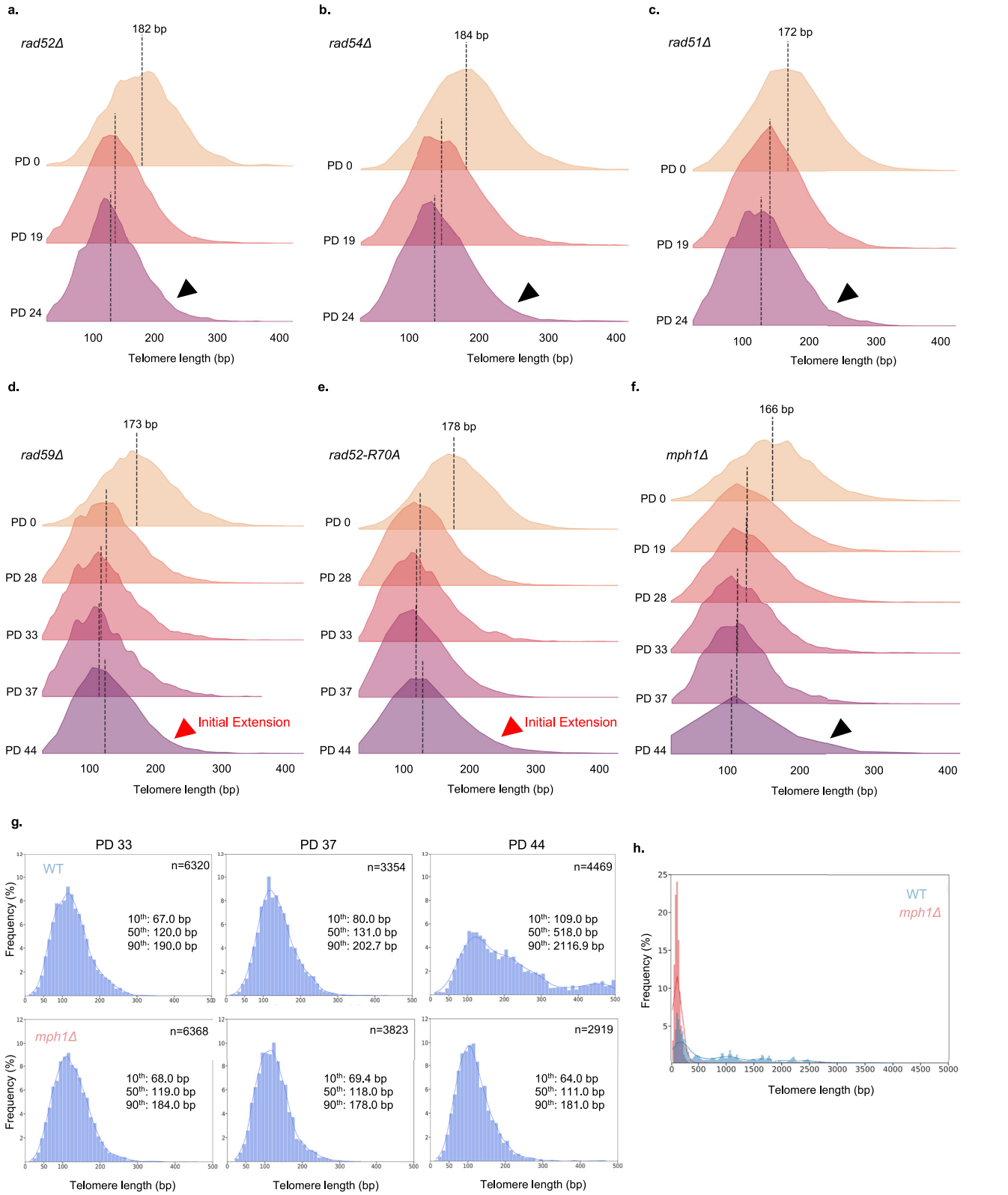

Fig. 2 | Genetic control of telomere extension. a–**f** Telomere length dynamics during ALT establishment in indicated BIR mutants. Black arrowheads mark telomeres populations that lack both initial and final telomere extensions ($p = 1$ for *rad51Δ*, *rad52Δ*, *rad54Δ*, and *mph1Δ*) (*rad51Δ* PD 19 $n = 1388$, PD 24 $n = 1457$; *rad52Δ* PD 19 $n = 5538$, PD 24 $n = 1863$; *rad54Δ* PD 19 $n = 854$, PD 24 $n = 509$; and *mph1Δ* PD 33 $n = 956$, PD 37 $n = 730$;). Red arrowheads mark telomeres populations that have initial extension but no evidence of final extension ($p = 5.59 \times 10^{-85}$ for *rad52-R70A* PD 37 $n = 1127$ vs PD 44 $n = 1344$; and $p = 9.39 \times 10^{-16}$ for *rad59Δ* PD 37 $n = 1460$ vs PD 44 $n = 2648$). Dotted lines: median telomere lengths. In all panels representative data from one of two biological repeats are shown. See also Supplementary Figs. 3, 5, 6, and Supplementary Data 2 for additional repeats and details. **g** Detailed comparison of telomere dynamics between WT and *mph1Δ* at PD 33, 37, 44 demonstrates that *mph1Δ* is defective (at PD 44) for both initial and final extensions. Telomere lengths are broken into 10 bp bins. **h** Direct comparison of telomere length distributions between WT and *mph1Δ* at PD 44. Telomere lengths are broken into 25 bp bins. In (**g**, **h**), representative data from one of two biological repeats are shown.

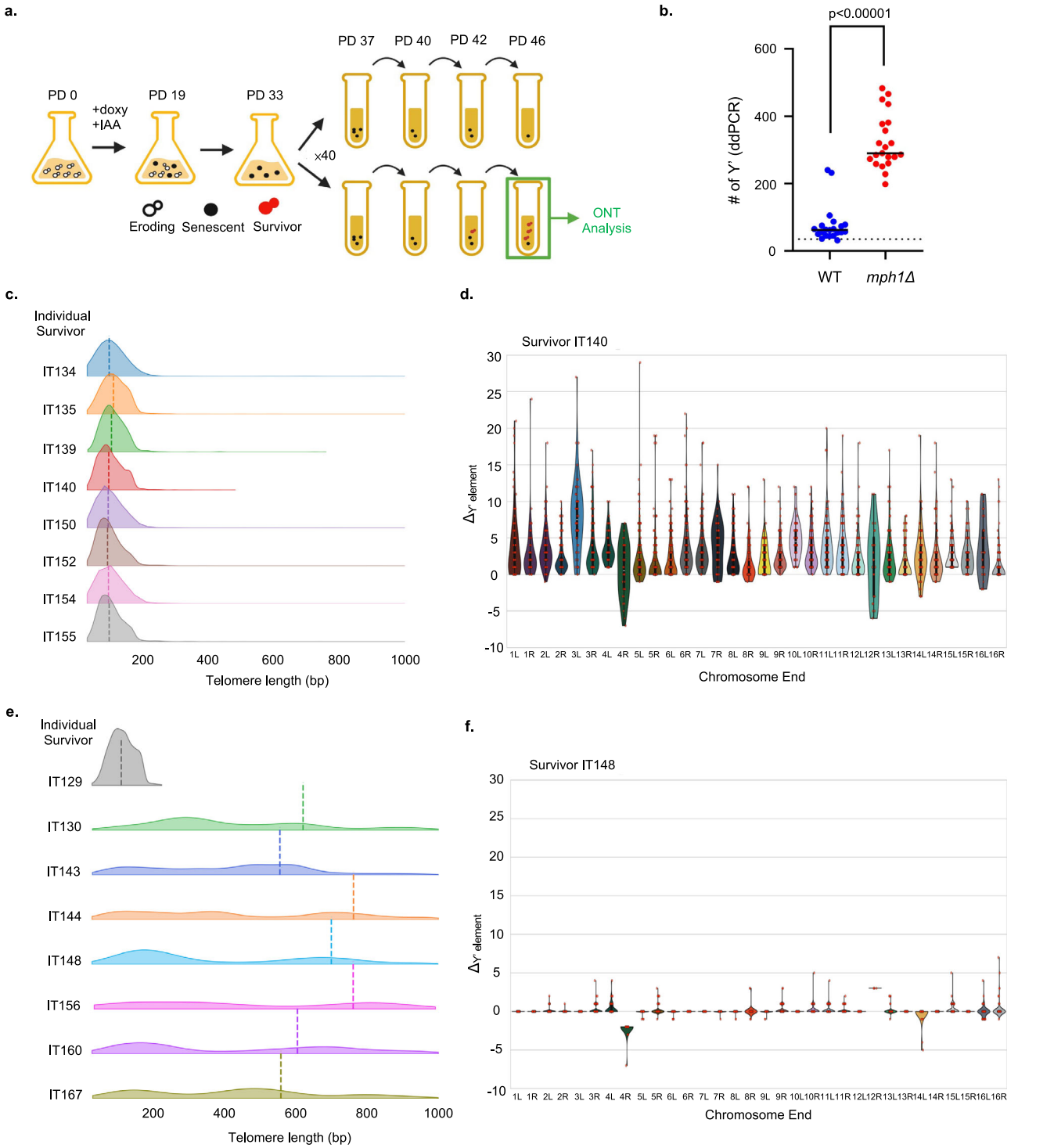

elements compared with WT (Fig. 4a). Also, WT sequencing reads with gains of ≥2 Y′ elements frequently mapped to Y′ elements located on different chromosome ends in the reference genome, suggesting the occurrence of template switching during acquisition of these sequences (Fig. 4b, Supplementary Fig. 8c, d, and Supplementary Data 4). This type of template switching was observed in 20.9% of WT cases that underwent acquisition of ≥2 Y′ elements (Fig. 4b, Supplementary Fig. 9a, and Supplementary Data 5) but was significantly reduced in *mph1Δ* cells (Fig. 4b, Supplementary Fig. 9b, c, and Supplementary Data 6).

The increased ability of *mph1Δ* cells to acquire multiple Y′ elements with less template switching suggests that the absence of Mph1 allows DNA synthesis during BIR to proceed more efficiently and with fewer interruptions through Y′-containing chromosome ends, consistent with what was previously described in BIR model systems[38–41]. Consistent with this notion, ONT sequencing analysis of recombination sites at sub-telomeric regions at PD 28 and PD 33 indicated the successful acquisition of Y′ elements in WT usually resulted from events initiated by invasion inside the interstitial telomere sequence (ITS) located immediately proximal to the acquired Y′ elements (Fig. 4c and Supplementary Fig. 8e, f). Although less common, some Y′ element acquisitions were initiated further away from the telomere—inside the X element or beyond. Notably, the fraction of recovered recombination events initiated beyond ITS sequences was significantly higher in

Fig. 3 | *mph1Δ* forms only unstable survivors with expanded Y′ arrays and short telomeres. a Study design to obtain independent ALT survivors by passaging cells in liquid cultures. To obtain independent survivors, cultures were split into multiple (~40) tubes at PD 33 and transferred at a low cell density every 24 h until the survivor formed (~PD 46). Independent survivors were analyzed by ONT sequencing and TeloTracker. Created in BioRender. Withers, K. (2026) https://BioRender.com/j3gg5ca. **b** The copy number of Y′ elements determined by ddPCR in individual survivors obtained from (**a**). Dotted line: number of Y′ elements in the parental (AM6991) strain. Solid line: median number of Y′ elements in survivors; $p < 1.00 \times 10^{-15}$ determined by two-sided Mann-Whitney U test. 21 biologically independent ALT survivors were collected for both WT and *mph1Δ*. Source data are provided as a Source Data file. **c** Analysis of telomere lengths by ONT sequencing in independent *mph1Δ* survivors shows short telomeres. Dotted lines: median telomere lengths. Y-axis: the frequency of correspondent telomere lengths for each independent survivor. **d** High and variable number of Y′ elements on individual chromosome ends in *mph1Δ* survivors. (The representative survivor IT140 from (**c**) is shown). Y-axis: the change (magnitude and direction) of the Y′ numbers between reads for individual chromosome ends in the survivor from the parental strain (AM7172). Each red dot represents an individual read, and the internal box plot shows the median (white line), interquartile range (box; 25th–75th percentiles), and whiskers extending to 1.5x the interquartile range. One survivor is shown; see Supplementary Fig. 7b, c for additional examples. Source data are provided as a Source Data file. **e** Analysis of telomere lengths by ONT sequencing in individual WT survivors shows long telomeres. Full telomere length distributions are shown in Supplementary Fig. 9d, including telomeres >1000 bp. Dotted lines: median telomere lengths. **f** Same as (**d**) but for the WT survivor IT148 from (**e**) from the parental strain AM6991. One survivor is shown; see Supplementary Fig. 7d for an additional example. Source data are provided as a Source Data file.

mph1Δ cells (34% of the cases) relative to WT (18%) (Fig. 4c and Supplementary Fig. 8e, f).

From the aforementioned observations, we propose three conclusions regarding the initial steps of ALT establishment. First, telomere erosion, initiated after telomerase inactivation, leads to extensive resection of chromosome ends that often proceeds beyond telomeres and Y′ elements, reaching pre-Y′ element regions, and activating large sub-telomeric regions for HR. Second, in the absence of Mph1, BIR synthesis initiated in distant sub-telomeric areas has a higher probability of reaching the end of the chromosome. Finally, HR proceeding by BIR plays a significant role in chromosome dynamics after telomere shortening and resection of chromosome ends, particularly when template switching is reduced.

Initial telomere extension is driven by homology

Considering our finding that extensive chromosome end resection activates large sub-telomeric regions for HR, we next investigated the properties of inter-telomeric recombination. Previously, it was proposed that recombination between yeast telomeres is driven exclusively by microhomology, owing to the irregularity of telomere repeats in yeast[2,3]. To test this, we identified the positions where recombination was initiated (hereafter, "initiation point") during the first telomere extensions by determining the points where telomeric sequences diverged between ALT survivors and the reference genome (similar to[24–26]; Supplementary Fig. 10). We observed that the initiation points on individual chromosomes used for the initial telomere extensions were often conserved among independent ALT survivors (Fig. 4d and Supplementary Data 7). A particular example is that the left arm of chromosome I (1 L) shared the same 36-bp telomere sequence before the initiation point (basal telomere sequence) in 15 of 19 independent WT survivors obtained from 3 independent experiments (Fig. 4d and Supplementary Data 7), suggesting that the initial extension of this arm often started from the same nucleotide position relative to the beginning of the telomere sequence. Several other chromosome ends, such as 2 L, 4 L, 10 L, 12 L, 13 L, and 13 R, also had a chromosome-specific initiation point (Fig. 4d and Supplementary Data 7). Notably, we identified that the telomere sequences proximal to the initiation point from every chromosome end shared significant homology (50 to 100 bp) with sequences located on several other chromosome ends (Supplementary Data 8), pointing to significant homology and suggestive of chromosome-end-specific HR. In fact, the ALT survivor's telomeres (both basal and diverged regions) shared homology with several reference telomeres, identifying them as potential donors (see example in Fig. 4e). Together, our results suggest that initial repair of eroded chromosome ends during ALT is initiated by HR, usually at preferred positions of homology, and can involve both telomeric and sub-telomeric regions.

To determine whether homology-based recombination alone can produce ALT survivors, we applied a population genetics modeling approach (Fig. 4f–h), which was built on the following assumptions: (1) telomere shortening occurs at an average rate of ~6 bp per telomere per cell division until at least one telomere reaches the critically short length threshold[21]; (2) a telomere reaching this threshold stops cell division and initiates long resection that exposes telomeres and pre-telomeric regions (X and Y′ elements); (3) the exposed telomeric and pre-telomeric regions can participate in HR; and (4) the 3′ ssDNA formed during resection can only invade unresected chromosomal regions. The results of this computational modeling suggested that HR involving telomeres and sub-telomeric regions can significantly delay cellular senescence (Fig. 4f) and promote the acquisition of numerous Y′ elements (Fig. 4h). However, HR alone was not sufficient to promote telomere extension and generate survivors (Fig. 4g), eventually generating population-wide senescence.

Stable ALT survivors are produced by copying telomeric circles

To explain how cells acquire long telomeres and escape senescence, we hypothesized that the elongation of telomeres may occur through the copying of telomere circles (t-circles), which are known to be present in human ALT cells, although it remains unclear whether they play any role in promoting ALT in humans[7,9,11,47,48]. Indeed, our population genetics model (Fig. 5a–c) predicted that copying from t-circles would lead to the formation of long telomeres, even when t-circles were used as templates by resected telomeres at frequencies as low as 1×10^{-5} per recombination attempt (Fig. 5b). Moreover, the model predicted that copying from t-circles would not only initiate telomere lengthening but also limit the acquisition of multiple Y′ elements at chromosome ends (Fig. 5c). Finally, the model indicated that telomere lengthening by copying from t-circles would restore the population's full dividing potential and the stable maintenance of chromosome ends, forming stable survivors with long telomeres (Fig. 5a).

To test this model empirically, we used ONT sequencing to analyze 15 independent WT survivors obtained by passaging in liquid cultures, and we found that the majority of these survivors had very long telomeres—some reaching >3,000 bp—and a low number of Y′ elements (Fig. 3e, f and Supplementary Fig. 9d). We noticed that 3 of 15 sequenced survivors contained recurring unusual nucleotides (for example A or C within TG-rich telomeres) at somewhat varying intervals (Fig. 5d). Such recurring mutations suggest that these telomere ends may have formed by copying from a t-circle, and the variable distance between mutations was indicative of instability during synthesis, prompting us to further characterize chromosome end structures in the survivors. To accomplish this, we manually analyzed the telomere sequences of all survivors for repetitive patterns and determined that telomeres in every WT survivor consisted of a single recurring telomere repeat ("unit") that varied between 88 and 168 bp in length (Figs. 5e, 6a, Supplementary Fig. 11a, b, 12, 13, and Supplementary Data 9–17). For example, survivor IT148 contained a total of 140 copies of a 136-bp unit that was tandemly repeated across its 12 homogeneous chromosome ends (Fig. 6a, Supplementary 11a, and Supplementary Data 9). The other chromosome ends were

https://doi.org/10.1038/s41467-026-72032-4

a.

# of Y' elements		WT	*mph1Δ*	
Start (reference)	Gained (ONT read)	# of reads (%)	# of reads (%)	
0	1	1190 (88.1%)	343 (75.7%)	
	≧2	160 (11.9%)	110 (24.3%)	p<0.00001
1	1	383 (59.6%)	150 (40.1%)	
	≧2	260 (40.4%)	224 (59.9%)	p<0.00001
2+	1	81 (45.8%)	44 (42.7%)	
	≧2	96 (54.2%)	59 (57.3%)	

b.

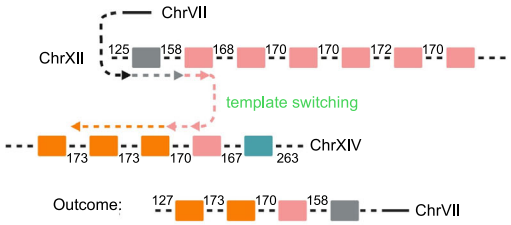

	No Template Switching	Template Switching
WT	383 (79.1%)	101 (20.9%)
mph1Δ	325 (86.9%)	49 (13.1%) p=0.00298

c.

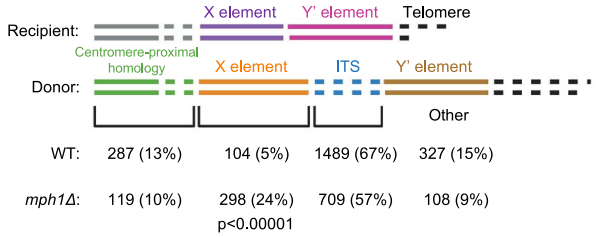

d.

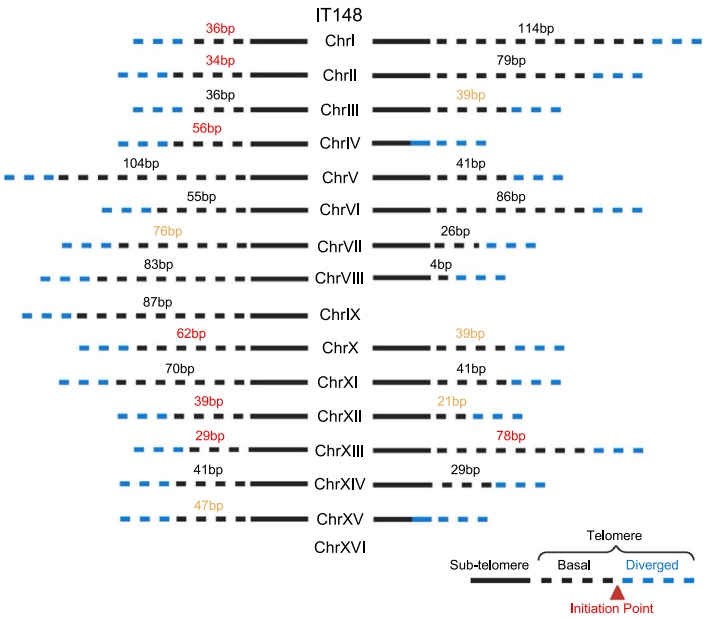

e.

f.

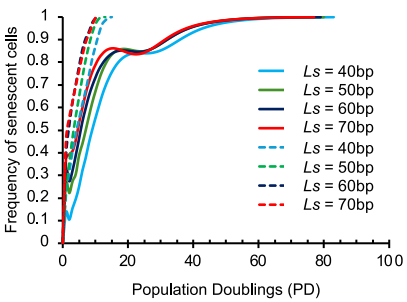

g.

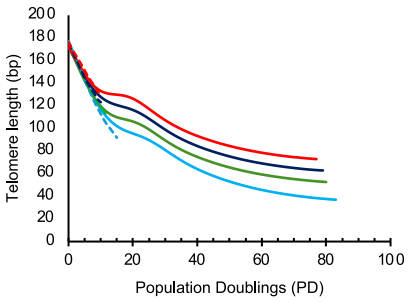

h.

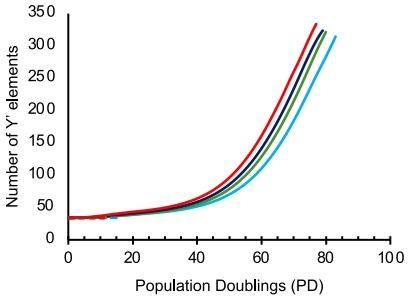

characterized by heterogeneity among ONT reads mapping to the same chromosome ends, suggestive of a continuing evolution of these ends. Following further stabilization by isolating a single-colony, we established that the stabilized derivative (named IT181) contained a total of 242 copies of the same 136-bp unit observed in the initial survivor across its 25 homogeneous ends (Fig. 5e and Supplementary Data 10).

If ALT survivors synthesize telomeres from a t-circle, we would expect the presence of t-circles within the cells to be detectable[48,49]. To test this, we performed rolling circle amplification (RCA) with φ29 polymerase in the absence of any primers on DNA samples purified from three independent ALT survivors (Fig. 5f and Supplementary Fig. 11c). Slot blots showed relatively strong hybridization to a telomere-specific probe in samples of all three survivors in the presence of φ29 in comparison to those without φ29, while WT cells at PD 0 did not show any significant signal in either condition (Fig. 5f and Supplementary Fig. 11c). To further support that the increased signal was from products of copying of a t-circle we performed denaturing

Fig. 4 | Homologous recombination in sub-telomeric and telomeric regions. **a** The number of Y′ elements gained during ALT establishment detected in individual ONT reads of cell populations at PD 28 and PD 33 combined. The number of reads with gains of ≥2 Y′ is higher ($p = 1.40 \times 10^{-10}$ (top); 2.08×10^{-9} (bottom), as determined by two-sided Chi-square test) in *mph1Δ* than in WT; see Supplementary Data 3. **b** Gains of ≥2 Y′ are often associated with template switching (TS). Top: example of TS in WT. Y′ colors are the same as in Fig. 1a. Numbers correspond to the lengths of interstitial telomere sequences (ITSs). Bottom: The frequency of TS in *mph1Δ* among reads with ≥2 Y′ gains is lower than in WT ($p = 0.00298$ by two-sided Chi-square test); see Supplementary Data 5, 6. **c** Recombination positions in sub-telomeres identified by ONT sequencing in reads with a gain or change in the first centromere-proximal Y′; donor positions divided into four regions: ITS, X element, centromere-proximal homology, and other. Significant increase of events in X element region ($p < 1 \times 10^{-15}$ by two-sided Chi-square test) in *mph1Δ* as compared to WT. **d** Positions of recombination between telomeres identified by ONT sequencing in WT ALT survivors (survivor IT148 shown as an example) as the junctions between the parental basal regions (black dashed lines) and the survivor diverged regions (blue dashed lines). The numbers indicate the length of the basal telomeres for each initiation point; red: HR initiation point shared between survivors from different experiments; yellow: shared between survivors within one experiment; black: unique to the survivor. **e** Example of alignment between a telomere of a survivor and its possible donor sequences from parental telomeres. Alignment divergences are labeled in red. **f**–**h** Computational modeling of telomere erosion, senescence, and repair by HR after telomeres reach a critically short length (*Ls*). Based on *Ls* between 60 and 70 bp[21] or even shorter[29], telomere dynamics for the range of *Ls* 40–70 bp was investigated. Telomeric HR was only allowed to occur between identified homologies (see Supplementary Data 8 and text for details). Dashed lines: no recombination; continuous lines: HR can occur between resected (< *Ls*) and non-resected chromosome ends (≥ *Ls*). **f** The onset and frequency of senescence. **g** Telomere length dynamics. **h** Y′ element copy number dynamics.

gel electrophoresis on the RCA products. Most of the hybridization signal was concentrated at >10 kb (Supplementary Fig. 11d, e), consistent with prior reports that detected RCA products from partially double-stranded telomeric circles[49,50]. Together, the presence of repetitive units in all analyzed survivors supports their formation through copying from t-circles, which were directly detected in these cells.

Interestingly, telomere reads with recurring telomere units, similar to those in established survivors, were clearly detected in PDs preceding survivor formation (as early as PD28) and indicated that t-circle copying had already begun (Supplementary Data 18). Importantly such reads were found 53x more often in WT compared to *mph1Δ* in early PDs (PD 19 through PD 37). This suggests the formation of early precursors of stable survivors as early as PD28, and that this occurs less frequently in cells lacking Mph1.

Copying t-circles is highly mutagenic

ONT analysis demonstrated that the repeating units on long telomere ends contained multiple mutations, including small insertions, deletions, and base substitutions, indicative of highly mutagenic DNA synthesis involved in their formation (Fig. 5e, g). There were also frequent insertions of non-unit telomeric sequences. For example, we detected 262 mutations across all repeated units of IT181 combined, which amounts to 8×10^{-3} mutation events/bp assuming independence of all mutation events (Supplementary Data 10). Mutation frequencies calculated for all three independent survivors and their derivatives were similar, ranging from 3×10^{-3} to 1×10^{-2} (Supplementary Data 19).

Further characterization of mutations detected in survivor IT181 showed that 72/262 mutations (27%) were single-base substitutions comprising either thymine (T)-to-guanine (G) or G-to-T transversions, and 188/262 (72%) were insertions/deletions also consisting of T and G (Fig. 5e, g and Supplementary Data 10). The remaining mutations consisted of one T-to-A transversion and one single-base A insertion. Mutation patterns for the two other WT survivors and their derivatives were similar to those observed in IT181, and the results obtained by ONT sequencing were also confirmed by PacBio sequencing. (Supplementary Figs. 11a, b, 12, 13, 14 and Supplementary Data 9–17; see Methods for details). Such high mutation frequencies and mutation spectra suggested that these mutations likely resulted from template switching or polymerase slippage that occurred during t-circle copying, which can be promoted by secondary structure formation. In addition, other replication problems including translesion DNA synthesis or the low fidelity of the replication machinery could also contribute to this mutagenesis. The idea of template switching is supported by the uneven distribution of mutations among repeated units. For example, in IT181 only 27% of repeated units contained mutations and the majority (77%) of the detected mutations were clustered in groups of 2 or more mutations within 10 bp distance, and a similar pattern was observed in other survivors (Supplementary Data 19). Each mutation cluster could in principle result from a single template switching event to a new position within the t-circle template, leading to a frameshift resulting in several mutations at a time. However, even considering formation of a mutation cluster as one concerted event, the mutation frequencies in the survivors remain high (between 2×10^{-3} and 7×10^{-3}).

To explore the origin of mutations identified in the repeated telomere units, we conducted phylogenetic and pairwise divergence analyses for mutated units in individual original survivors (IT148, IT130, and IT160). The phylogenetic analysis produced a star phylogeny pattern, with few or no clades supported by high bootstrap values (Supplementary Fig. 15a–c), suggesting that the mutations in each of these original survivors likely originated from independent copying of a single, survivor-specific, ancestral t-circle. In agreement with this notion, pairwise divergence analysis showed a unimodal distribution in IT148 and IT130 (Supplementary Fig. 15d, e), suggesting that most mutations found in these survivors occurred independently in each unit. The presence of the additional pairwise divergence peaks in IT160 (Supplementary Fig. 15d, e) might indicate that some of the mutations resulted from recombination between chromosome arms instead of copying from t-circles, although it is most likely that the majority formed independently. Additional pairwise divergence peaks were detected in several survivor derivatives as compared to their parental survivors (Supplementary Fig. 16), which suggests that secondary transferring between chromosome arms likely occurred during survivor stabilization.

Based on the report that a sufficient length, usually >100 bp, is needed for DNA bending[51], we hypothesized that template switching facilitates telomere lengthening during the first telomere extension, and that this event might promote the formation of t-circles. Indeed, when we included the potential for template switching at microhomologies within telomeres in our computational model (Fig. 6b–d), which previously considered only HR, we observed elongation of telomeres extending beyond 100 bp (Fig. 6d). Additionally, the model predicted that such template switches would significantly delay or even prevent the onset of senescence (Fig. 6b). In this model, however, template switching might not be sufficient to generate stable survivors. In support of the validity of this computational model, we observed that the sequence of the 136-bp t-circle unit that gave rise to IT148 contained several repeats of TGTGTGGGTGTGG, and the formation of the repeating unit could be explained by several rounds of template switching that occurred prior to t-circle formation (Fig. 6e). Similar repeats were identified within t-circle units in other ALT survivors (Fig. 6a). Together, we propose that initial telomere extension is promoted by interruptions in BIR repair synthesis followed by re-invasion/re-annealing at microhomologies within telomeres, and that this initial telomere extension is important for generating t-circles, which, in turn, are required for generating stable ALT survivors.

https://doi.org/10.1038/s41467-026-72032-4

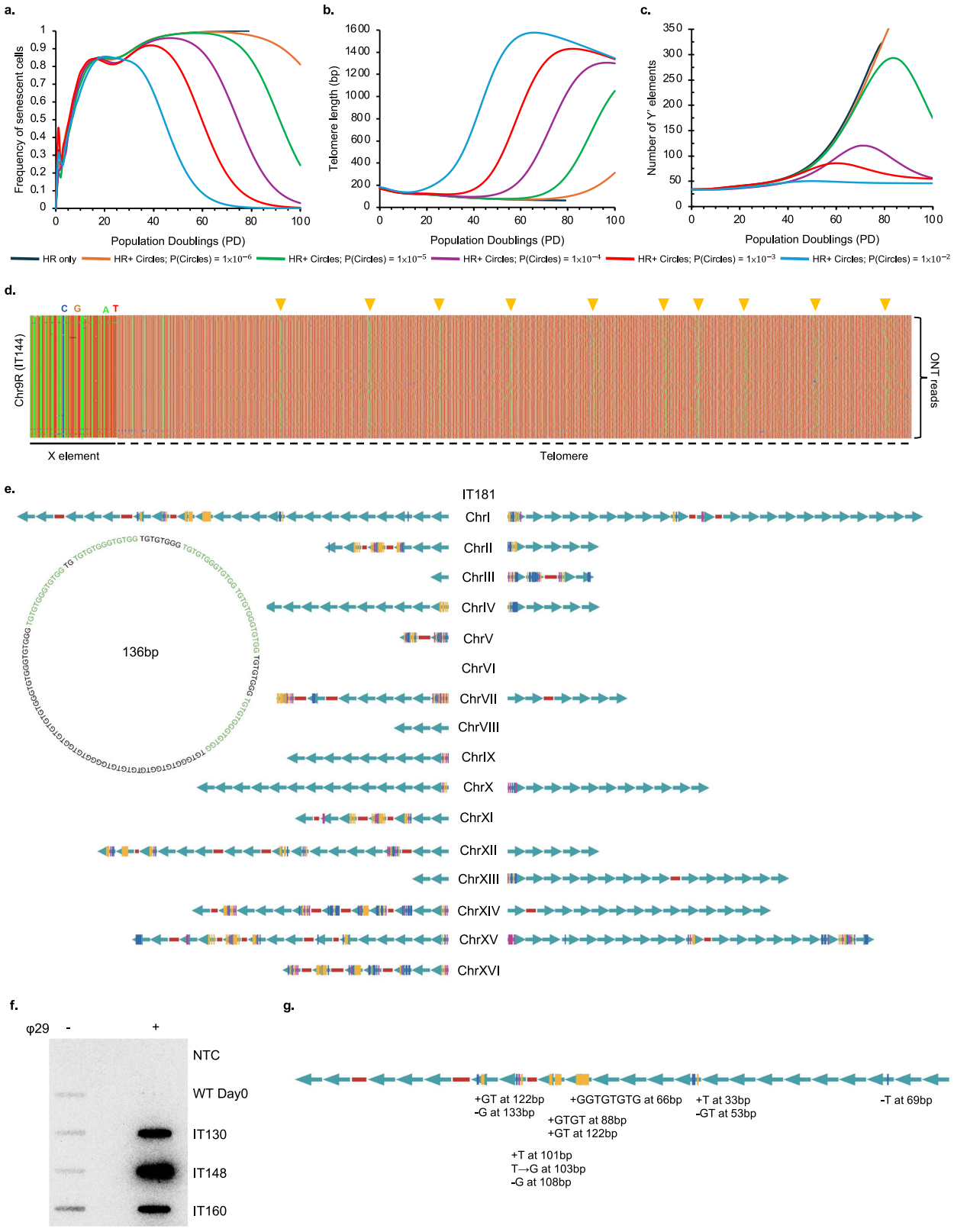

Finally, we modified our computational simulations by including the potential for HR, template switching at microhomologies, and the generation and copying from t-circles at varying probabilities. Although HR alone could not prevent population senescence (Fig. 7ai), allowing template switching at microhomologies allowed the formation of unstable (Type I) survivors with a high number of Y′ tandem repeats and short telomeres (Fig. 7aii). These cell populations, however, were heterogeneous, unstable, and never regained full survivorship. Only when the potential to generate and copy from t-circles—even at very low frequencies—was included did the model predict rapid formation of stable (Type II) or hybrid (containing both long tandem repeats of Y′ elements and long telomeres[21]) survivors (Fig. 7aiii).

https://doi.org/10.1038/s41467-026-72032-4

Fig. 5 | Highly mutagenic copying of telomeric circles forms long telomeres. **a**–**c**. Computational modeling of telomere erosion, senescence, and repair using HR with *Ls* = 60 when the model includes the possibility of copying from t-circles. Copying of t-circles is assumed to add 2 kb of telomeric sequences. Colors indicate probabilities of copying from t-circles; dark blue line: HR of resected with unresected telomeres with no copying from t-circles (as in Fig. 4f–h). **a** Onset and frequency of senescence. **b** Telomere length dynamics. **c** Y′ element copy number dynamics. **d** Alignment of ONT sequencing reads of chromosome arm 9 R in survivor IT144 demonstrates sequence periodicity. Yellow arrows denote periodical non-canonical adenines (green A) in the new telomere sequence. **e** Highly mutagenic copying of a t-circle by each chromosome end forms long telomeres in ALT survivors. Survivor IT181 is shown with the schematic of its 136-bp t-circle (unit) presented on the left. Teal arrow: one unit sequence; horizontal red lines: non-circle telomere sequences; vertical ticks: mutations introduced during copying of the units (yellow: insertions; blue: deletions; pink: base substitutions). Only regions with sufficient ONT coverage from homogeneous chromosome arms are shown. (See Supplementary Figs. 11a, b, 12, 13 and Supplementary Data 9–17 for other examples and details). **f** t-circles detected by rolling circle amplification (RCA) followed by slot blot analysis with hybridization to a telomere-specific probe. Source data are provided as a Source Data file. **g** High-resolution representation of mutations in chromosome arm 1 L of IT181 from (**e**).

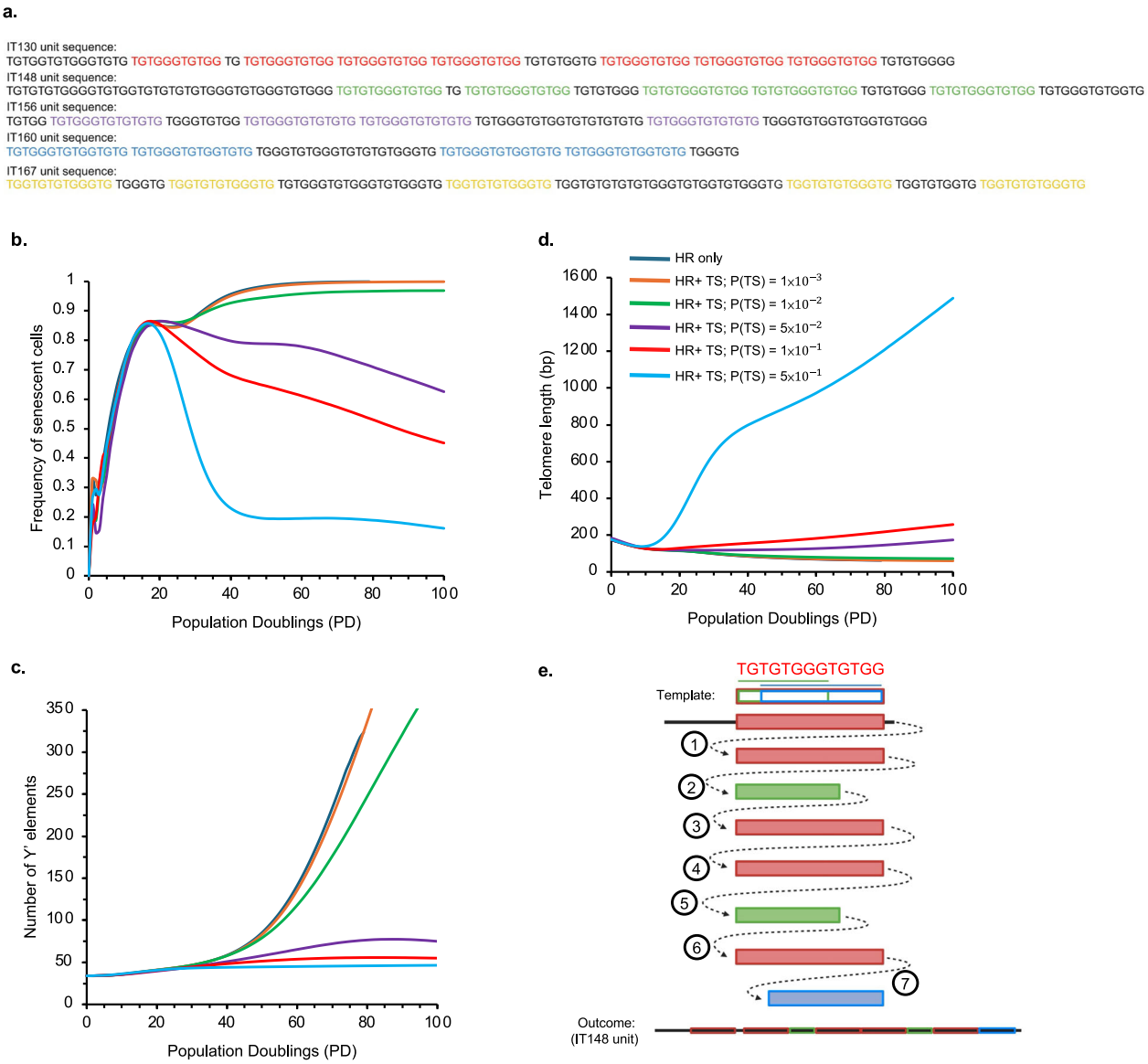

Fig. 6 | Template switching at microhomologies promotes initial telomere extension. **a** Examples of t-circle unit sequences from different survivors from Fig. 3e. The colored sequences denote iterations inside the units, indicative of the unit's formation by template switching (TS). **b**–**d**. Computational modeling of telomere erosion, recombination, and ALT survivor formation using HR when the model includes the possibility of TS with *Ls* = 60. Dark blue line: HR of resected with unresected telomere and without template switching (as in Fig. 4f–h). Colors represent different probabilities of TS at telomeres following initial HR. **b** Onset and frequency of senescence. **c** Y′ element copy number dynamics. **d** Telomere length dynamics. **e** Schematic of template switching proposed to generate the t-circle unit in IT148. The arrows and numbers indicate the TS events and their order, respectively.

https://doi.org/10.1038/s41467-026-72032-4

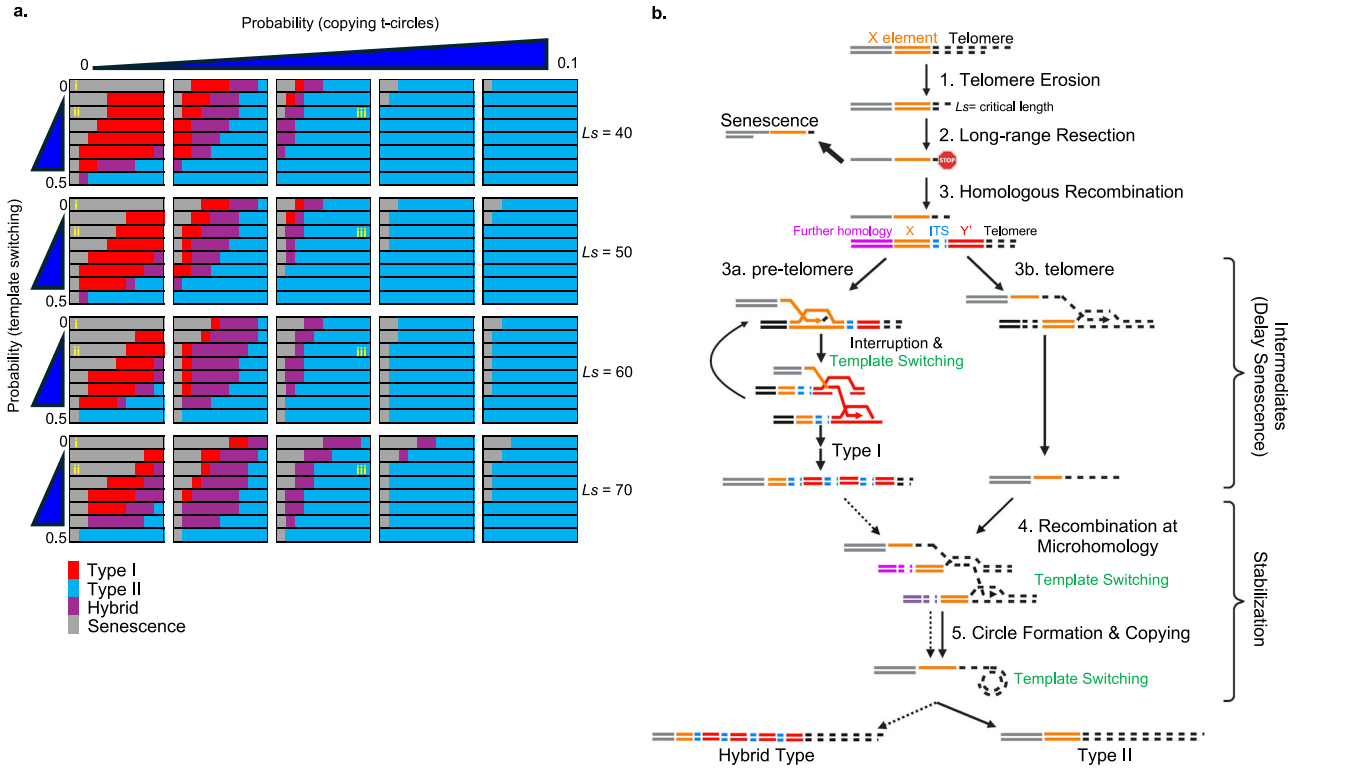

Fig. 7 | Models of ALT establishment. a Computational modeling of ALT survivor formation using HR combined with variable probabilities of template switching and copying from t-circles. For each combination of parameters, the relative frequency of outcomes after PD 100 is shown. Outcomes are classified as Type I, Type II, or Type I/Type II hybrid based on the number of Y′ elements and the length of telomeres at PD 100; a "dead population" indicates frequency of senescence > 0.9999. Results are shown for four different telomere length thresholds to activate senescence (40, 50, 60, and 70 bp). **b** Molecular model showing the main steps of ALT establishment described in detail in the text. Note: Starting from Step 4, only the intermediate without Y′ tandems is shown since the steps of telomere extension are similar for the intermediate with Y′ tandems. Created in BioRender. Withers, K. (2026) https://BioRender.com/j8w9hsi.

Discussion

Here, using ONT sequencing and computational modeling, we identified molecular milestones of ALT establishment, including the delay of cellular senescence by HR via BIR, an initial telomere extension enabled by recombination at microhomologies, and a final telomere extension leading to stable ALT survivor formation by copying of t-circles. We also determined that the copying of telomeric circles is highly mutagenic and that Mph1, a homolog of human FANCM that facilitates template switching, plays an important role throughout ALT establishment.

Molecular model of ALT establishment in yeast

We propose a model (Fig. 7b) where telomere erosion leads to the formation of critically short telomeres, initiating extensive chromosome end resection. This resection proceeds into sub-telomeric regions, consistent with[52,53] but often exceeds 10 kb advancing into Y′ elements, X elements, and other centromere-proximal regions and making these areas active initiators of repair for the resected chromosome ends (Figs. 7b-2). This potentiates homology-based recombination of the entire exposed ssDNA regions with non-resected chromosome ends, either at telomeres or within pre-telomeric regions (Fig. 7b-3). When HR by BIR occurs within pre-telomeric regions, it often leads to the acquisition of one or more Y′ elements (Fig. 7b-3a), eventually producing unstable intermediates bearing Y′ tandem repeats but short telomeres. Similarly, BIR between telomeres does not lead to telomere extension sufficient to produce ALT survivors (Fig. 7b-3b). Instead, these early homology-based recombination events, at telomeric and sub-telomeric regions, delay the onset of cellular senescence, providing an opportunity for later steps required for ALT survivor formation. Interestingly, our experimental data and computational model suggest the possibility of competition between Y′ element amplification and telomere elongation; however, additional studies are needed to test this further.

Following initial HR, the first telomere extension is promoted by recombination at microhomologies, including template switching (Figs. 7b-4). Critically, template switching can extend telomeres beyond the threshold required for DNA bending[51]—which could be necessary for the formation of t-circles. Subsequently, copying of t-circles enables the formation of very long telomeres that halt accumulation of Y′ elements, quickly leading to the emergence of stable survivors (Figs. 7b-5).

While the mechanism of t-circle production remains unclear, our study demonstrates that t-circles are both generated and used as templates for copying during ALT establishment in *S. cerevisiae*. In mammalian cells, the accumulation of t-circles serves as an important indicator of cells with established ALT[11,47,48,54,55], though their role in ALT establishment and maintenance remains undetermined. Similarly, while t-circles were described in relation to ALT in budding yeast[49,56], their specific role as repair templates remained unclear. The use of t-circles as templates was recently proposed to explain the repair of dysfunctional telomeres in budding yeast, although this mechanism was not linked to ALT, and no t-circles were identified[57]. Previous studies performed in *Kluweromyces lactis* detected repeats of 50- to 150-bp-long units in ALT survivor telomeres, suggestive of t-circle copying[58–60]. However, since the experiments were performed by Southern blot analysis, the mechanism underlying this copying and the level of associated mutagenesis were not determined. Unlike the "roll and spread" model proposed by studies in *K. lactis*, in which a single

chromosome is extended by t-circle copying and is subsequently used as a template for other chromosomes[58–60], our result suggests that, at least initially, chromosome arms copy the same unit independently.

Our data demonstrate that t-circle copying is highly mutagenic. This could be explained by high level of template switching which is known to occur frequently during BIR[11,55,61,62], which could be further promoted by secondary structures formed by telomere repeats (e.g., G4 quadruplexes). In addition, the high level of mutagenesis might also result from other replication problems, including polymerase slippage, translesion DNA synthesis, or decreased fidelity of the replication machinery. Though the precise mechanism of mutagenesis during ALT is not yet fully understood, our study represents the first estimation of the level of mutations associated with telomere extension during ALT establishment.

Our study also uncovered that Mph1 plays an important role in ALT establishment, and see also refs. 43,44. In particular, we observed that only unstable ALT survivors—representing a fluctuating population of intermediates—were formed in the absence of Mph1, while the formation of long telomeres characteristic of stable ALT survivors was extremely rare. Mph1 interrupts BIR synthesis, whereas synthesis in *mph1Δ* cells more easily traverses through long, continuous stretches of Y' tandem repeats, frequently copying through the chromosome ends; for this reason, *mph1Δ* cells are characterized by a higher frequency of repaired resected chromosomes compared with WT, which would explain the higher frequency of survivors in *mph1Δ* compared with WT cells. This interpretation is supported by reports that *mph1Δ* cells are characterized by fewer interruptions and fewer template-switching events during BIR in other DSB repair models[38–41]. The same characteristic of *mph1Δ* might also be responsible for the observed defect in the formation of stable survivors with long telomeres, as it is possible that template switching at microhomologies might be needed for the initial telomere elongation, for the formation of t-circles and/or for the utilization of t-circles as templates for synthesis. Besides the known role of Mph1 in BIR template switching, its other functions described in the context of normal DNA replication—for example, activities involved in fork reversal or DNA damage bypass[63,64] —may also influence ALT.

Future studies

Our study in yeast demonstrates that extensive DNA resection initiates HR in sub-telomeric regions, and that this recombination precedes and affects ALT development. We therefore predict that the specific structure of pre-telomeric regions, including the number of Y' elements and their organization in tandems, might significantly affect the genetic control and frequency of ALT outcomes, which should be systematically investigated in the future. Similarly, the effects of initial telomere lengths on ALT outcomes in various yeast strains should be investigated.

In this study we observed that DNA resection makes both sub-telomeric and telomeric areas available for recombination in yeast. If resection is similar in other species, pre-telomeric regions would be predicted to play important roles in those organisms as well. However, in humans, telomeres are significantly longer, and senescence is activated when telomeres are of significant length[65–69], warranting specific research considering our results in yeast. It is possible that only telomeric regions will be resected, but resection of chromosome ends in humans may sometimes reach sub-telomeric regions and produce Type I-like outcomes, similar to those observed in mouse embryonic stem cells following telomerase inactivation[70,71].

The repeat regularity of human telomeres makes them a perfect substrate for HR, which might efficiently extend cell survival and even elongate telomeres. Thus, ALT in human cells may not require template switching via microhomology, even though template switching has been proposed to occur during ALT[11,55]. Given the length of telomeres at senescence, it could also be that long resected ssDNA repeats would produce t-circles in human cells more frequently than in yeast, and this would explain the preponderance of Type II survivors during ALT in humans[11,72].

Based on our finding that Mph1 promotes ALT in yeast, future studies should evaluate the potential role of its human homolog FANCM. Several studies have highlighted the important role of FANCM in ALT maintenance in humans, and it was shown that FANCM depletion in ALT-positive cells resulted in decreased cellular viability, increased replication stress, higher levels of TERRA, and an increase in ALT-associated PML bodies (APBs)[73–75]. It is possible that these phenotypes may result from overly processive BIR[38,40,76], which is similar to what we observed in *mph1Δ* mutants promoting the formation of Type I ALT survivors. Other studies have reported increased accumulation of t-circles in the absence of FANCM, which might indicate that FANCM is required for utilizing telomeric circles as HR templates during ALT and requires further investigation.

Most importantly, our finding that yeast telomeres are extended by copying t-circles motivates future studies to determine whether telomeric circles in humans also serve as templates for DNA synthesis contributing to the extension of ALT telomeres. However, the regularity of human telomeres currently precludes direct testing of this hypothesis and necessitates the development of specialized experimental systems to enable such studies in human cells.

Methods

Strains

The genotypes of all yeast strains used in this study are shown in Supplementary Data 20. Two experimental systems to study ALT in yeast were used. The AM3692 (telomerase elimination system) was constructed by ref. 21 with the following genotype: *MATa/α ura3-Y1/ura3-Y1 ade5-y7/ade5-y7 HPHMX/HPHMX crl3–2/crl3–2 trp-Y1/ trp-Y1 leu1-Y1/leu1-Y1 TLC1/tlc1::BSD*.

The AM6991 (telomerase shut-off) was constructed using *tetO2-TLC1*[22,27] that we received from Dr. Raymund Wellinger and Dr. Maria Teixeira with the following genotype: *MATa ade2 lys2 trp1 ura3 his3 his5 leu2-Δ1* tetO2(*TLC1*)-*KANMX*. To ensure the complete elimination of telomerase, the following changes were introduced in this strain. First, *tetO2-TLC1* was transformed with plasmid containing *OsTIR1-URA3*[77] to produce AM6396. Next, an auxin-induced degron (AID-*HPHMX*) was inserted into *EST2* right before its stop codon to produce AM6749. Finally, tetO2(*TLC1*)-*KANMX* was changed to tetO2(*TLC1*)-*NATMX* to create AM6991. Addition of doxycycline into the growth medium suppressed *TLC1* expression, while addition of IAA resulted in elimination of the telomerase catalytic subunit (Est2).

All single-gene deletion mutants were constructed by transformation with a PCR-derived *KANMX*, *NATMX*, or *HPHMX* module, each flanked by sequences homologous to the regions surrounding the open reading frame of each gene[78,79]. All constructs were confirmed by PCR and by phenotype. The *rad52-R70A* and *pif1* mutants (*pif1-m2* and *pif1-NLSΔ*) were constructed by CRISPR using the oligos and plasmids described in refs. 35,80.

Media and growth conditions

Rich medium, Yeast extract-peptone-dextrose (YEPD), and other media were prepared as described in ref. 81. Antibiotics, including hygromycin, nourseothricin, G418, and blasticidin, have been added to YEPD as described in ref. 81. Synthetic complete medium with bases and amino acids omitted (e.g. SC-Ura) were prepared as described in ref. 81. Sporulation media were prepared with potassium acetate (2% w/v KAc). All yeast cultures were grown at 30 °C.

Determining ALT frequencies by plating

To determine ALT frequencies in the telomerase-elimination system, AM3692 and the derivatives of AM3692, cells were sporulated, tetrads were dissected, and individual meiotic outcomes (selected by markers)

were passaged in liquid YEPD followed by plating on YEPD plates[21]. The frequencies of ALT survivors were calculated by plating a known number of these cells and identifying how many survivors formed as described in ref. 21.

To determine ALT frequencies in the new telomerase shut-off system, AM6991 and the derivatives of AM6991, cells were grown in liquid YEPD overnight to reach ~10^7 cells/mL (PD 0) and then passaged at 100 cells/mL in 5 mL liquid YEPD containing doxycycline (30 μg/mL) and IAA (100 μM). In experiments using AM6991 and its mutant derivatives, we plated 500 cells on each YEPD agarose plate with both doxycycline and IAA addition after the fifth passage. For the cell cultures entering senescence earlier (*rad52Δ*, *rad51Δ* and *rad54Δ*), we plated the same number of cells after the third passage. For the cells with longer telomeres including *pif1-NLSΔ*, *pif1-m2*, and *rif1Δrif2Δ*, we plated the same number of cells after the ninth passage. Emergent survivors on plates were confirmed by the maintenance of growth after streaking for single cells on fresh YEPD agarose plates with the same concentration of chemicals, and ALT frequencies were calculated by the number of survivors formed divided by the total number of plated cells as described in ref. 21.

Following ALT establishment in yeast liquid cultures

To follow ALT establishment in the telomerase shut-off system, AM6991 and the derivatives of AM6991, cells were grown in 250 mL of liquid YEPD overnight to reach 10^9 cells in total (PD 0). Cells were passaged at 100 cells/mL in liquid YEPD containing doxycycline and IAA (250 mL to 2 L). For mutants with increased or decreased ALT frequency, the number of cells at later passages was adjusted. Cells with deletions of *RAD52* or *RAD54* were kept in YEPD-doxy-IAA media for additional 2 days to confirm that no survivors were formed in these cultures. For each time point, we collected at least 10^9 cells in total for the extraction of the high molecular weight (HMW) DNA used for ONT library preparation. Once cell populations reached PD 33, 500 cells per tube were transferred into 40 tubes of 5 mL liquid YEPD-IAA-doxycycline media and the same passages continued every 24 h until the formation of independent survivors.

RNA extraction and RT-qPCR quantification of *TLC1* expression

Cultures of AM6991 (WT) were grown in liquid YEPD overnight to ~1×10^7 cells/mL (PD 0) and passaged at 100 cells/mL in liquid YEPD (with or without 30 μg/mL doxycycline) every 24 h for 8 days. A total of 1×10^7 cells were pelleted by centrifugation for each biological replicate at Day 0 (PD 0), Day 4, and Day 8 and frozen at −80 °C until extraction. Total RNA was extracted from frozen samples using a MasterPure ™ Yeast RNA Purification Kit with DNase I treatment for 10 minutes. Samples were additionally treated with 10 units of DNase I (NEB) treatment for 30 min at 37 °C to remove contaminating gDNA, then cleaned by phenol-chloroform-isoamyl alcohol extraction and ethanol precipitation. RNA yield was quantified by Qubit™ RNA High Sensitivity Assay Kit (Invitrogen) and quality assessed by Qubit™ RNA Integrity and Quality Assay Kit (Invitrogen).

A total of 1 μg total RNA per sample was used as a template for duplicate cDNA reactions with the Protoscript® II First Strand cDNA Synthesis Kit (NEB). RNA templates were incubated with 6 μM Random Primer Mix for 5 min at 65 °C, then kept on ice for the addition of Protoscript II Reaction Mix and Protoscript II Enzyme Mix, except in the case of No-RT negative control samples, in which the enzyme mix was replaced by nuclease-free water. All reactions were incubated at 25 °C for 5 min, then 42 °C for 60 min, followed by inactivation at 80 °C for 5 min.

Reactions of Power SYBR® Green PCR Master Mix were prepared with 500 nM primers (for the reference gene *SSY1* (FW: GTCCAGGGCAACTAGGAAATAC; RVS: CTGTGAGTCCAAACCCAAGTAG) and for *TLC1* (DG293: AATGGCTGTTGCGTTTGCTT; DG294: ACCACAAATTGCGCACACAC)[82]) and 2 μL of diluted (1:3) cDNA as template. Samples were run on a QuantStudio 3™ (Applied Biosystems) as follows: initial denaturation at 95 °C for 10 min, followed by 50 cycles of 95 °C for 15 s and 60 °C for 1 min with a ramp rate of 1.6 °C per second and one fluorescence acquisition per cycle. A melt curve analysis was performed after cycling to ensure amplification specificity, using the following steps: 95 °C for 15 s, 60 °C for 1 min, a dissociation step with acquisitions during the 0.1 °C per second ramp to 95 °C, then a hold at 4 °C after completion. Cycle threshold values were exported using the Applied Biosystems Design & Analysis Software version 2.8.0. Expression of *TLC1* was normalized to expression of reference gene *SSY1*[83] for each sample, then expressed as fold change in expression relative to the mean expression of YEPD PD 0 samples following the $2^{-\Delta\Delta Ct}$ method.

Droplet-digital polymerase chain reaction (ddPCR) to quantify Y′ element copy number

Genomic DNA was extracted by a glass bead-phenol-sodium dodecyl sulfate protocol[84] from ALT survivors grown in YEPD-IAA-doxycycline liquid medium, and the DNA concentration was measured by Qubit dsDNA HS Assay Kit (Invitrogen). 10 ng of DNA was digested with 20 units of XhoI at 37 °C to separate Y′ tandems located at chromosome ends[21]. After digestion, DNA samples were diluted 10 to 100-fold to optimize Y′ number measurements. *ACT1*, which is present in a single copy in haploid strains, was used as a reference for copy number (FW: GCCTTCTACGTTTCCATCCA; RVS: GGTAGAGAGAAACCAGCGTAAA). Primers specific to Y′ elements were designed in the region shared by all Y′ elements (FW: TGGTAGCGGTTCACAAAGAG; RVS: CCTTCACTCTCCAACTTCTCTG). The number of positive droplets containing targeted sequence (*ACT1* or Y′) was quantified using the QX200 Droplet-digital PCR system (BioRad) according to manufacturer's recommendations. The total number of Y′ in each sample was calculated as described in ref. 21.

Analysis of chromosome end structures using Oxford Nanopore Technologies (ONT) sequencing

To prepare yeast genomic DNA libraries for ONT sequencing, we collected a total of 1–3 × 10^9 yeast cells and extracted HMW DNA as described in ref. 21. For the TeloTag library preparation, we followed the established protocol described in ref. 45. For the TeloTracker library preparation, we used the Q20 + ONT ligation kit (Oxford Nanopore Technologies SQK-LSK114) with the following modifications. 3–4 μg of HMW DNA were mixed with Ultra II end-prep and the FFPE DNA repair mix (New England Biolabs), then incubated the reactions at 20 °C for 30 min, followed by at 65 °C for 30 min. Next, we incubated our samples with SRE XL buffer (PacBio) on a tube rotator for 20 minutes at room temperature. After centrifugation at 20,000 × *g* for 30 min, the pellet was washed with 80% ethanol and dissolved in EB buffer. Once the DNA was fully dissolved, we ligated the samples with ONT adapters for 30 minutes at room temperature. Lastly, we washed the pellet with long fragment buffer (LFB) and dissolved the DNA in EB buffer.

We measured the DNA concentration using Qubit dsDNA HS Assay Kit (Invitrogen) and loaded ~500 ng of DNA sample for each ONT sequencing run. Samples were run on a PromethION flow cell (R10.4.1) using the PromethION 2 Solo for 3–72 hours to acquire 3–5 Gb per sample and were operated using MinKNOW software (v.24.11.10). To enrich for telomere reads during sequencing, we performed adaptive sampling to deplete any reads corresponding to the "internal chromosomal sequences" (located more than 70 kb away from chromosome ends). By selecting against reads that aligned with the sequences in the reference, we achieved a 3 to 5-fold enrichment for the telomere sequences.

Telomere length determination using PacBio sequencing

PacBio sequencing was performed by the University of Washington PacBio Sequencing Services. The procedure included multiplexing the

genome library followed by PippinHT size selection above 15 kb and sequencing using a Sequel II SMRT Cell 8 M with 30-hour movie, yielding an average output of 30 Gb of reads for each pooled sample with ~25 kb median read length.

TeloTracker bioinformatic analysis of ONT sequencing results and statistical analysis

All Oxford Nanopore reads were basecalled using Dorado's *sup* model without adapter trimming. Reads were subsequently filtered to retain long, high-quality reads (read length > 2000 bp; $Q \geq 10$).

Parental references. A reference genome for the WT strain (AM6991) was generated de novo using Flye and Medaka, followed by manual inspection using IGV. Reference genomes for the *mph1Δ* strains (AM7172 and AM7302) were generated in a similar manner, using the AM6991 reference genome as the starting point. Chromosome-end features—including telomeric, subtelomeric, and unique chromosome-end "anchor" sequences—were annotated for each reference genome using a combination of manual inspection and custom Python scripts. Phylogenetic Neighbor-Joining trees for Y′ and X elements were constructed using MEGA (alignment with MUSCLE; 10,000 bootstrap replicates; bootstrap cutoff of 90).

Analysis of telomere length. All samples were analyzed using a custom Python package, TeloTracker. Briefly, TeloTracker maps reads to specific chromosome ends by BLASTn alignment to unique chromosome-end "anchor" sequences. Reads mapping to a single chromosome end ("anchored reads") were subsequently analyzed to determine whether they reached the chromosome end. Specifically, TeloTracker identifies nanopore adapter sequences using Porechop and determines telomeric sequence presence and length using custom Python scripts. Only reads containing both a nanopore adapter sequence and a terminal telomeric tract of at least 30 bp were classified as telomere reads and included in downstream analyses. Notably, the 10th percentile of telomere lengths in the population was experimentally determined to be a relatively stable value for mutant cells unable to extend telomeres (e.g. *rad52Δ*, *rad51Δ*, and *rad54Δ*) and was therefore used as an estimate of the length of telomeres at which cells enter senescence (*Ls*).

Initial telomere extension. For each telomerase shut-off time course experiment, we performed a Mann–Whitney U test to compare the distributions of longest 25% of telomere lengths in the current PD population of cells with the longest 25% of the immediately preceding PD. The Mann–Whitney U comparisons were performed to test a null hypothesis that there was no telomere extension versus an alternative hypothesis that telomere lengths significantly increased in the current PD relative to the previous one. The first PD showing a statistically significant increase in telomere lengths ($p < 0.05$) was designated as the PD at which initial telomere extension occurred. Time courses lacking statistically significant initial telomere extension were classified as having no initial telomere extension.

Sub-telomeric recombination analysis. For each strain, an initial sub-telomeric analysis was performed to quantify Y′ elements in each telomere-containing read using BLASTn. Additional sub-telomeric analyses were performed using TeloTracker for strains AM6991, AM7172, and AM7302, using their respective annotated reference genomes. First, Y′ elements were classified according to their closest matching reference Y′ using RepeatMasker. Next, pre-Y′ recombination sites were identified in reads that had gained a Y′ element or exhibited a change in their most centromere-proximal Y′. To map these recombination sites, the pre-Y′ region was subdivided into three components: the pre-X element, the X element, and the ITS. If no recombination breakpoint could be identified, the recombination site was assigned to the ITS if at least one of the candidate donor chromosome ends contained an ITS in its reference sequence. All remaining pre-Y′ recombination events were classified as Other/Unknown. In addition, to identify template switching between Y′ elements, the full Y′ structure of each read was manually compared to the corresponding reference sequences.

Analysis of Y′ element mapping accuracy from individual reads. We assessed the accuracy of Y′ element assignment using the current Y′ element group definitions (Fig. 1a; Supplementary Fig. 9a–c; see also the "Parental references" section above). To estimate the frequency of "errors" in the assignment of Y′ elements, we analyzed individual reads at PD 0 and applied the same workflow we employed to identify template switching events from PD 28 and PD 33 (Fig. 4a–c and Supplementary Fig. 8). Because the frequency of recombination events between Y′ elements at PD 0 is very low (Supplementary Fig. 7h), we expected that the Y′ element sequences should always match the reference, while mismatches would allow us to estimate the frequency of "errors" in assignment of Y′ elements. The results of this analysis initially showed that the frequency of misassigned Y′ elements at PD 0 was 1.5% in both WT and *mph1Δ* cells, which is substantially lower compared with the frequencies of template switching detected at PD 28 and PD 33. In addition, we noticed that among 1.5% of errors detected by the analysis of PD 0, misalignments between particular Y′ elements were overrepresented. Specifically, misalignment was more frequently found between the first Y′ element at chromosome arm 14-L, which was originally marked in light blue in Fig. 1a, and two Y′ sequences shown in dark blue (the Y′ elements at 7-R and 16-L). Therefore, we decided to exclude template-switching events between them from our analysis. Following their exclusion, the level of errors calculated from misassigned Y′ elements at the PD 0 were 0.4% (Supplementary Fig. 8d and Supplementary Data 4), which is substantially lower than the corrected frequencies of template switching for PD28 and PD33 (combined).

Survivor reference analysis. Samples from ALT survivors were first analyzed for Y′ element distribution and telomere length as described above. Survivors containing chromosome ends with stable Y′ copy numbers and long telomeres (> 1000 bp) were selected for reference construction, and a reference sequence was generated for each chromosome end using Flye. References that did not yield a single consensus sequence were inspected manually and reconstructed with manual intervention when possible. Successfully generated references with high read coverage (> 10×) were manually examined for repeated sequence patterns (units) indicative of copying from telomeric circles. The mutation frequency for each survivor was calculated as the total number of mutations detected in that survivor divided by the total number of base pairs across all units from the survivor. When sequence resolution was not achievable, the corresponding chromosome end was classified as heterogeneous.

Population and individual-read telomere circle analysis. Populations of strains AM6991, AM7172, and AM7302 were analyzed to identify circular telomeric sequences (units). Long telomeric reads (> 300 bp) were manually inspected for repeated sequence patterns indicative of copying from telomeric circles.

Statistical analysis. All statistical analyses were performed with GraphPad and TeloTracker.

Phylogenetic analysis of repeating telomeric units in stable WT survivors

Phylogenetic relationships among repeating telomeric units were inferred using the UPGMA method[85], as implemented in MEGA11[86], with pairwise deletion and the Kimura two-parameter model applied to

distance calculations[87]. Bootstrap support values were obtained from 1,000 replicates. In addition, pairwise distance relationships between units were calculated using MEGA11.

Extraction and detection of telomeric circle DNA

Extraction of circular DNA was performed from 1×10^9 cells by first incubating in 0.75 M sorbitol, 75 mM EDTA, and 0.7% 2-mercaptoethanol with 2.5 mg/mL Zymolyase (MP Biomedicals) at 37 °C for 90 minutes. Protoplasts were pelleted and treated with the Qiagen Plasmid Plus Midiprep Kit (Qiagen) as in ref. 88 with the following modifications: samples were centrifuged at 3900 × *g* for 10 min to remove cell debris before passage through a QIAfilter Midi cartridge, and washing with buffer ETR was omitted. Samples were eluted with buffer EB and further concentrated by ethanol precipitation with 1/10 volume sodium acetate pH 7.0, and 75 µg GlycoBlue™ co-precipitant at −20 °C for 60 min, followed by centrifugation at 15,000 × *g* for 30 min and washed with 70% ethanol. Samples were resuspended in buffer EB and kept at 4 °C. Samples were digested with 20 units of EcoRI (NEB) for 16 hours at 37 °C to linearize mitochondrial DNA and fragment any contaminating gDNA. Samples were cleaned by phenol-chloroform-isoamyl alcohol extraction, then ethanol precipitated in the presence of co-precipitant as described above. Resulting samples were quantified by Qubit™ DNA High Sensitivity Assay Kit.

Rolling circle amplification was performed using the Phi29-XT RCA Kit (NEB) without primers. All samples were normalized to 20 ng input DNA per reaction and incubated for 16 h at 42 °C, then 65 °C for 10 min. Two biological replicates were performed for each strain. Samples were diluted with 2 parts RCA: 15 parts 2X SSC and loaded onto a 2X SSC pre-soaked positively charged Hybond-N+ nylon membrane (Cytiva) with a PR 648 slot blot manifold (Cytiva), followed by UV exposure to crosslink DNA to the membrane. Aliquots of the same samples were loaded on a denaturing gel (1% agarose, 30 mM NaOH, 2 mM EDTA), run at 35 V for 24 h, and capillary transferred onto a Hybond-N+ membrane as described[89]. To detect telomeric RCA products, probe synthesis was performed using the RadPrime DNA Labeling System (Invitrogen) with the following reagent modifications: 2.5X RadPrime Buffer without random octamers (125 mM Tris-HCl pH 6.8, 12.5 mM $MgCl_2$, 25 mM 2-mercaptoethanol) was substituted for provided RadPrime Buffer, addition two custom oligos (IDT DNA), 3 µg KR247: CACCCACACACCACACCCAC, and 25 ng of template telomeric 88-mer KR244: TGTGGGTGTGGTGTGTGTGGGTGTGGTGTGTGGGTGTGGGTGTGTGTGGGTGTGTGGGTGTGGTGTGTGTGGGTGTGGTGTGTGGGTG. The reaction was stopped by addition of 200 µL distilled water, incubation at 100 °C for 5 minutes, and snap cooling on ice 1 minute prior to usage. Hybridization was performed as follows: membranes were pre-hybridized with hybridization buffer (0.25 M sodium phosphate buffer pH 7.2, 5% SDS, 1 mM EDTA pH 8.0) at 65 °C for 10 min, followed by hybridization in the same buffer with 50 µL of probe solution for 24 h. Membranes were washed three times with low-stringency wash buffer (2X SSC, 0.1% SDS at 65 °C), exposed to a GEO Phosphor screen for 4 h, and then imaged using an Azure Sapphire Biomolecular Imager.

Computational modeling of yeast populations undergoing telomere erosion and repair

We developed a computational model of telomere dynamics that simulates telomerase-negative populations of cells, with telomere shortening (erosion), senescence, and potential recovery (formation of ALT survivors from post-senescence cells) based on fully stochastic population genetics principles in finite populations. As in Kockler et al.[21], our model mimics a case where each telomere of every dividing cell erodes, and replicative senescence is activated when the shortest telomere in a cell reaches a critically short threshold length. Senescent cells, on the other hand, are allowed to recombine through multiple modalities (see below), which can potentially lead to cells in which all telomeres surpass the critical length threshold, leading to resumption of cell cycling. Additional to telomere repeats, our model considers pre-telomeric regions, which play important roles in cell dynamics and formation of ALT survivors when senescent cells are allowed to recombine. Notably, our simulations track all per-chromosome-end features for each cell in the population, thus allowing us to capture the full heterogeneity and dynamics over time of chromosome-end structures within and between cells. Also, our computational model allows the following of very large populations—approximating realistic experimental cell populations—which enables the identification of critical dynamics caused by very low frequency events that would be missed when investigating smaller populations. Because the modeling is based on directly following every cell and every telomere structure within each cell in a population and not on mathematical inferences, it naturally restricts properties of cell division and chromosome-ends to biologically relevant ranges and allows the inclusion of complex modes of recombination.

General chromosome-end properties and population processes. Our simulations start with a cell with 32 chromosome ends (16 chromosomes), each characterized by a telomere repeat, possible Y′ elements, an X element, and a pre-Y′/X elements region. The average telomere length as well as the number and distribution of Y′ elements across chromosome ends is based on that of the sequenced strain under study. As in Kockler et al.[21], the model follows exponential growth of this ancestral cell, with telomeres randomly increasing or decreasing in length every cell division to generate a large and heterogeneous population prior to telomerase inactivation.

When modeling of telomerase-negative cell populations begins, one randomly chosen cell from the pre-evolved population is used as starting point per replicate, and the study of multiple replicates allows capturing variation in dynamics due to differences in initial telomere length composition. Populations expand exponentially, and cell properties are analyzed every PD. Simulations also mimic the experimental design with passages (sub-samples of the cell pool) at specific PDs. For every PD, population expansion is based on randomly choosing cells one by one from the whole pool of N cells, either non-senescent or senescent, until $2N$ cells are achieved. This approach adds random genetic drift as well as heterogeneity to division rates among non-senescent cells, which simulates observations from microfluidics experiments of telomerase-negative single cell lineages[22]. If the chosen cell is non-senescent, it divides creating a daughter cell, with telomere shortening occurring on both the parent and the daughter cells independently on all chromosomes. Shortening follows an average of n nucleotides per chromosome end per division, with each chromosome eroding one of the two telomeres (chosen at random) with Poisson-distributed average $2n$ nucleotides to follow end-replication properties. If a chosen cell is senescent, with one or more chromosome ends shorter than a threshold length (Ls), we apply either death (removed from the pool of cells with probability P_{death}) or recombination (1-P_{death}).

Recombination in senescent cells. During the replication process, if a senescent cell is chosen, it cannot divide, but it can attempt recombination. The model assumes that chromosome ends with telomeres shorter than Ls go through long-distance 5′-3′ end resection, generating ssDNA at these chromosome ends that can only find homology with dsDNA of non-resected chromosome ends (with telomeres longer than Ls). It also assumes that end resection will regularly extend beyond the telomere repeat region, which is supported by our current genomic data and previous studies showing multiple instances of Y′ element swapping[21,25]. Therefore, our recombination scheme allows resected chromosome ends to recombine through HR at either

telomeric repeats or at sub-telomeric regions, including X and Y′ elements when present. For each resected chromosome, the model first identifies the element that will attempt HR. As a simplifying assumption, we assign equal probability of HR along the resected chromosome end to the telomere repeat, each individual Y′ element (if any) and the X element. When an X element is assigned for recombination, it randomly chooses among the X elements of non-resected chromosome ends for HR, capturing the X element and terminal regions (Y′ elements and telomere repeats) of the donor chromosome end. When a Y′ element is chosen for recombination, HR occurs with a Y′ element randomly chosen among all the Y′ elements present in non-resected chromosome ends of the cell, capturing all terminal regions of the donor chromosome end (terminal Y′ elements, if any, and the telomere repeat).

When recombination is assigned to a resected telomere repeat, the model allows for HR between telomere repeats or between the repeats and t-circles, if present, the latter with probability $P_{\text{t-circle}}$ for each recombination attempt. We also incorporate the possibility that recombining resected telomeres can engage in subsequent recombination events through a model equivalent to template switching by microhomology with other non-resected donor telomere ends based on probability P_{ts}. When template switching occurs, the terminal end of the ssDNA telomere repeat randomly identifies a location along the donor telomere, extending the length of repeats. If template switching occurs, the model further allows for additional template switches (each with probability P_{ts}), with a maximum of 5 consecutive switches. Finally, our model investigates the potential impact of t-circles emerging from the dynamics of template switching at microhomologies following initial HR, where ssDNA telomeric repeat segments could be long enough to generate a t-circle[51]. This possibility allows the probability of recombination between telomere repeats and t-circles to be dynamic, starting with no t-circles and increasing as a senescent cell goes through recombination events, with each new t-circle adding $P_{\text{dyn-t-circle}}$ to $P_{\text{t-circle}}$. Each cell in the population, therefore, can have a different $P_{\text{t-circle}}$ that, on division, will be equally split between parent and daughter cells; therefore, survivor cells that successfully elongated telomeres with t-circles are predicted to reduce the number of t-circles over time.

Parameters. Unless otherwise noted, and to speed up the simulation process when following exponential growth for many PDs without passages, we limited the maximum number of cells to 2×10^7, at which point a very moderate subsampling (10%) is applied, which still allows capturing consequences of very low frequency events. We used an erosion rate per telomere per division of $n = 6$ based on Kockler et al.[21]. Previous genomic studies of telomere length and dynamics using long-read sequencing suggested the telomere length threshold (*Ls*) required to activate senescence to be between 60 and 70 bp[21], although analyses of single-cell lineages indicated *Ls* to be shorter[29]. We, therefore, considered telomere dynamics for the range of *Ls* between 40 and 70 bp. We also applied $P_{death} = 0.1$ unless otherwise noted. We considered 120 bp as the minimum ssDNA repeat length to generate a t-circle, and recombination with a t-circle added an average of 2000 bp of telomere repeats to the previously short telomere repeat. Our study followed dynamics for up to 100 PDs, and we considered a population under full terminal arrest when the fraction of senescent cells was greater than 0.9999. Results from all conditions analyzed were based on 200 independent population replicates, except for non-recombination conditions where 100,000 replicates were conducted due to much larger variances.

Reporting summary

Further information on research design is available in the Nature Portfolio Reporting Summary linked to this article.

Data availability

Requests for unique/stable reagents generated in this study and further information and resources should be directed to the corresponding author. All ONT sequencing generated in this study have been deposited in NCBI's BioProject with the accession code PRJNA1254968. Source data are provided with this paper.

Code availability

The code used to analyze the telomere sequencing data is available at GitHub (https://github.com/Jacob-M-Wells/TeloTracker)[90]. The code for the computational modeling of telomere dynamics is available at GitHub (https://github.com/josep-comeron/Yeast-Telomere-Dynamics)[91].

References

1. Bonnell, E., Pasquier, E. & Wellinger, R. J. Telomere Replication: Solving Multiple End Replication Problems. *Front Cell Dev. Biol.* **9**, 668171 (2021).
2. Wellinger, R. J. & Zakian, V. A. Everything you ever wanted to know about *Saccharomyces cerevisiae* telomeres: beginning to end. *Genetics* **191**, 1073–1105 (2012).
3. Teixeira, M. T. *Saccharomyces cerevisiae* as a Model to Study Replicative Senescence Triggered by Telomere Shortening. *Front Oncol.* **3**, 101 (2013).
4. De Lange, T. Telomere-related genome instability in cancer. *Cold Spring Harb. Symp. Quant. Biol.* **70**, 197–204 (2005).
5. Hemann, M. T., Hackett, J., A, I. J. & Greider, C. W. Telomere length, telomere-binding proteins, and DNA damage signaling. *Cold Spring Harb. Symp. Quant. Biol.* **65**, 275–279 (2000).
6. Neumann, A. A. & Reddel, R. R. Telomere maintenance and cancer - look, no telomerase. *Nat. Rev. Cancer* **2**, 879–884 (2002).
7. Dilley, R. L. & Greenberg, R. A. ALTernative Telomere Maintenance and Cancer. *Trends Cancer* **1**, 145–156 (2015).
8. Musmaker, K., Wells, J., Tsai, M. C., Comeron, J. M. & Malkova, A. Alternative Lengthening of Telomeres in Yeast: Old Questions and New Approaches. *Biomolecules* **14**, 113 (2024).
9. Zhang, J. M. & Zou, L. Alternative lengthening of telomeres: from molecular mechanisms to therapeutic outlooks. *Cell Biosci.* **10**, 30 (2020).
10. Cesare, A. J. & Reddel, R. R. Alternative lengthening of telomeres: models, mechanisms and implications. *Nat. Rev. Genet* **11**, 319–330 (2010).
11. O'Sullivan, R. J. & Greenberg, R. A. Mechanisms of Alternative Lengthening of Telomeres. *Cold Spring Harb. Perspect. Biol.* **17**, a041690 (2025).
12. Hu, J. et al. Antitelomerase therapy provokes ALT and mitochondrial adaptive mechanisms in cancer. *Cell* **148**, 651–663 (2012).
13. Lundblad, V. & Blackburn, E. H. An alternative pathway for yeast telomere maintenance rescues *est1*- senescence. *Cell* **73**, 347–360 (1993).
14. Le, S., Moore, J. K., Haber, J. E. & Greider, C. W. *RAD50* and *RAD51* define two pathways that collaborate to maintain telomeres in the absence of telomerase. *Genetics* **152**, 143–152 (1999).
15. Teng, S. C. & Zakian, V. A. Telomere-telomere recombination is an efficient bypass pathway for telomere maintenance in *Saccharomyces cerevisiae*. *Mol. Cell Biol.* **19**, 8083–8093 (1999).
16. Teng, S. C., Chang, J., McCowan, B. & Zakian, V. A. Telomerase-independent lengthening of yeast telomeres occurs by an abrupt Rad50p-dependent, Rif-inhibited recombinational process. *Mol. Cell* **6**, 947–952 (2000).
17. Lydeard, J. R., Jain, S., Yamaguchi, M. & Haber, J. E. Break-induced replication and telomerase-independent telomere maintenance require Pol32. *Nature* **448**, 820–823 (2007).
18. Huang, P. et al. *SGS1* is required for telomere elongation in the absence of telomerase. *Curr. Biol.* **11**, 125–129 (2001).

19. Johnson, F. B. et al. The *Saccharomyces cerevisiae* WRN homolog Sgs1p participates in telomere maintenance in cells lacking telomerase. *EMBO J.* **20**, 905–913 (2001).
20. Chen, Q., Ijpma, A. & Greider, C. W. Two survivor pathways that allow growth in the absence of telomerase are generated by distinct telomere recombination events. *Mol. Cell Biol.* **21**, 1819–1827 (2001).
21. Kockler, Z. W., Comeron, J. M. & Malkova, A. A unified alternative telomere-lengthening pathway in yeast survivor cells. *Mol. Cell* **81**, 1816–1829 e5 (2021).
22. Xu, Z. et al. Two routes to senescence revealed by real-time analysis of telomerase-negative single lineages. *Nat. Commun.* **6**, 7680 (2015).
23. Coutelier, H. et al. Adaptation to DNA damage checkpoint in senescent telomerase-negative cells promotes genome instability. *Genes Dev.* **32**, 1499–1513 (2018).
24. Chang, M., Dittmar, J. C. & Rothstein, R. Long telomeres are preferentially extended during recombination-mediated telomere maintenance. *Nat. Struct. Mol. Biol.* **18**, 451–456 (2011).
25. Churikov, D., Charifi, F., Simon, M. N. & Geli, V. Rad59-facilitated acquisition of Y' elements by short telomeres delays the onset of senescence. *PLoS Genet* **10**, e1004736 (2014).
26. Fu, X. H. et al. Telomere recombination preferentially occurs at short telomeres in telomerase-null type II survivors. *PLoS One* **9**, e90644 (2014).
27. Bah, A., Gilson, E. & Wellinger, R. J. Telomerase is required to protect chromosomes with vertebrate-type T2AG3 3' ends in *Saccharomyces cerevisiae*. *J. Biol. Chem.* **286**, 27132–27138 (2011).
28. Zeinoun, B., Teixeira, M. T. & Barascu, A. Hog1 acts in a Mec1-independent manner to counteract oxidative stress following telomerase inactivation in *Saccharomyces cerevisiae*. *Commun. Biol.* **7**, 761 (2024).
29. Rat, A., Martinez Fernandez, V., Doumic, M., Teixeira, M. T. & Xu, Z. Mathematical model linking telomeres to senescence in *Saccharomyces cerevisiae* reveals cell lineage versus population dynamics. *Nat. Commun.* **16**, 1024 (2025).
30. Shi, I. et al. Role of the Rad52 amino-terminal DNA binding activity in DNA strand capture in homologous recombination. *J. Biol. Chem.* **284**, 33275–33284 (2009).
31. Downing, B., Morgan, R., VanHulle, K., Deem, A. & Malkova, A. Large inverted repeats in the vicinity of a single double-strand break strongly affect repair in yeast diploids lacking Rad51. *Mutat. Res* **645**, 9–18 (2008).
32. Signon, L., Malkova, A., Naylor, M. L., Klein, H. & Haber, J. E. Genetic requirements for *RAD51*- and *RAD54*-independent break-induced replication repair of a chromosomal double-strand break. *Mol. Cell Biol.* **21**, 2048–2056 (2001).
33. Wilson, M. A. et al. Pif1 helicase and Poldelta promote recombination-coupled DNA synthesis via bubble migration. *Nature* **502**, 393–396 (2013).
34. Hu, Y. et al. Telomerase-null survivor screening identifies novel telomere recombination regulators. *PLoS Genet* **9**, e1003208 (2013).
35. Lee, R. S. et al. Identification of the nuclear localization signal in the *Saccharomyces cerevisiae* Pif1 DNA helicase. *PLoS Genet* **19**, e1010853 (2023).
36. Schulz, V. P. & Zakian, V. A. The saccharomyces *PIF1* DNA helicase inhibits telomere elongation and de novo telomere formation. *Cell* **76**, 145–155 (1994).
37. Piazza, A. et al. Stimulation of gross chromosomal rearrangements by the human CEB1 and CEB25 minisatellites in *Saccharomyces cerevisiae* depends on G-quadruplexes or Cdc13. *PLoS Genet* **8**, e1003033 (2012).
38. Jain, S., Sugawara, N., Mehta, A., Ryu, T. & Haber, J. E. Sgs1 and Mph1 Helicases Enforce the Recombination Execution Checkpoint During DNA Double-Strand Break Repair in *Saccharomyces cerevisiae*. *Genetics* **203**, 667–675 (2016).
39. Mehta, A., Beach, A. & Haber, J. E. Homology Requirements and Competition between Gene Conversion and Break-Induced Replication during Double-Strand Break Repair. *Mol. Cell* **65**, 515–526 e3 (2017).
40. Stafa, A., Donnianni, R. A., Timashev, L. A., Lam, A. F. & Symington, L. S. Template switching during break-induced replication is promoted by the Mph1 helicase in *Saccharomyces cerevisiae*. *Genetics* **196**, 1017–1028 (2014).
41. Stivison, E. A., Young, K. J. & Symington, L. S. Interstitial telomere sequences disrupt break-induced replication and drive formation of ectopic telomeres. *Nucleic Acids Res* **48**, 12697–12710 (2020).
42. Piazza, A. et al. Dynamic Processing of Displacement Loops during Recombinational DNA Repair. *Mol. Cell* **73**, 1255–1266 e4 (2019).
43. Silva, S. et al. Mte1 interacts with Mph1 and promotes crossover recombination and telomere maintenance. *Genes Dev.* **30**, 700–717 (2016).
44. Luke-Glaser, S. & Luke, B. The Mph1 helicase can promote telomere uncapping and premature senescence in budding yeast. *PLoS One* **7**, e42028 (2012).
45. Sholes, S. L. et al. Chromosome-specific telomere lengths and the minimal functional telomere revealed by nanopore sequencing. *Genome Res* **32**, 616–628 (2022).
46. Oganesian, L. & Karlseder, J. Mammalian 5' C-rich telomeric overhangs are a mark of recombination-dependent telomere maintenance. *Mol. Cell* **42**, 224–236 (2011).
47. Nabetani, A. & Ishikawa, F. Unusual telomeric DNAs in human telomerase-negative immortalized cells. *Mol. Cell Biol.* **29**, 703–713 (2009).
48. Henson, J. D. et al. DNA C-circles are specific and quantifiable markers of alternative-lengthening-of-telomeres activity. *Nat. Biotechnol.* **27**, 1181–1185 (2009).
49. Aguilera, P. et al. Telomeric C-circles localize at nuclear pore complexes in *Saccharomyces cerevisiae*. *EMBO J.* **41**, e108736 (2022).
50. Zellinger, B., Akimcheva, S., Puizina, J., Schirato, M. & Riha, K. Ku suppresses formation of telomeric circles and alternative telomere lengthening in *Arabidopsis*. *Mol. Cell* **27**, 163–169 (2007).
51. Vafabakhsh, R. & Ha, T. Extreme bendability of DNA less than 100 base pairs long revealed by single-molecule cyclization. *Science* **337**, 1097–1101 (2012).
52. Hackett, J. A. & Greider, C. W. End resection initiates genomic instability in the absence of telomerase. *Mol. Cell Biol.* **23**, 8450–8461 (2003).
53. Fallet, E. et al. Length-dependent processing of telomeres in the absence of telomerase. *Nucleic Acids Res* **42**, 3648–3665 (2014).
54. Cesare, A. J. & Griffith, J. D. Telomeric DNA in ALT cells is characterized by free telomeric circles and heterogeneous t-loops. *Mol. Cell Biol.* **24**, 9948–9957 (2004).
55. Zhang, T. et al. Break-induced replication orchestrates resection-dependent template switching. *Nature* **619**, 201–208 (2023).
56. Larrivee, M. & Wellinger, R. J. Telomerase- and capping-independent yeast survivors with alternate telomere states. *Nat. Cell Biol.* **8**, 741–747 (2006).
57. Dudragne, L., Garrido, C., Ilioaia, O., Bernardes, J. S. & Xu, Z. Transient telomere uncapping triggers telomeric and subtelomeric rearrangements. *EMBO Rep.* **27**, 1607–1631 (2026).
58. Natarajan, S. & McEachern, M. J. Recombinational telomere elongation promoted by DNA circles. *Mol. Cell Biol.* **22**, 4512–4521 (2002).
59. Natarajan, S., Groff-Vindman, C. & McEachern, M. J. Factors influencing the recombinational expansion and spread of telomeric tandem arrays in *Kluyveromyces lactis*. *Eukaryot. Cell* **2**, 1115–1127 (2003).

60. McEachern, M. J. & Haber, J. E. Break-induced replication and recombinational telomere elongation in yeast. *Annu Rev. Biochem* **75**, 111–135 (2006).
61. Anand, R. P. et al. Chromosome rearrangements via template switching between diverged repeated sequences. *Genes Dev.* **28**, 2394–2406 (2014).
62. Smith, C. E., Llorente, B. & Symington, L. S. Template switching during break-induced replication. *Nature* **447**, 102–105 (2007).
63. Zheng, X. F. et al. Processing of DNA structures via DNA unwinding and branch migration by the *S. cerevisiae* Mph1 protein. *DNA Repair (Amst.)* **10**, 1034–1043 (2011).
64. Schurer, K. A., Rudolph, C., Ulrich, H. D. & Kramer, W. Yeast *MPH1* gene functions in an error-free DNA damage bypass pathway that requires genes from Homologous recombination, but not from postreplicative repair. *Genetics* **166**, 1673–1686 (2004).
65. Baird, D. M., Rowson, J., Wynford-Thomas, D. & Kipling, D. Extensive allelic variation and ultrashort telomeres in senescent human cells. *Nat. Genet* **33**, 203–207 (2003).
66. Levy, M. Z., Allsopp, R. C., Futcher, A. B., Greider, C. W. & Harley, C. B. Telomere end-replication problem and cell aging. *J. Mol. Biol.* **225**, 951–960 (1992).
67. Karimian, K. et al. Human telomere length is chromosome end-specific and conserved across individuals. *Science* **384**, 533–539 (2024).
68. Schmidt, T. T. et al. High resolution long-read telomere sequencing reveals dynamic mechanisms in aging and cancer. *Nat. Commun.* **15**, 5149 (2024).
69. Sanchez, S. E. et al. Digital telomere measurement by long-read sequencing distinguishes healthy aging from disease. *Nat. Commun.* **15**, 5148 (2024).
70. Lee, H., Niida, H., Sung, S. & Lee, J. Haplotype-resolved de novo assembly revealed unique characteristics of alternative lengthening of telomeres in mouse embryonic stem cells. *Nucleic Acids Res* **52**, 12456–12474 (2024).
71. Sung, S., Kim, E., Niida, H., Kim, C. & Lee, J. Distinct characteristics of two types of alternative lengthening of telomeres in mouse embryonic stem cells. *Nucleic Acids Res* **51**, 9122–9143 (2023).
72. Atari, A., Jiang, H. & Greenberg, R. A. Mechanisms and genomic implications of break-induced replication. *Nat. Struct. Mol. Biol.* **32**, 1871–1882 (2025).
73. Pan, X. et al. FANCM, BRCA1, and BLM cooperatively resolve the replication stress at the ALT telomeres. *Proc. Natl. Acad. Sci. USA* **114**, E5940–E5949 (2017).
74. Pan, X. et al. FANCM suppresses DNA replication stress at ALT telomeres by disrupting TERRA R-loops. *Sci. Rep.* **9**, 19110 (2019).
75. Silva, B. et al. FANCM limits ALT activity by restricting telomeric replication stress induced by deregulated BLM and R-loops. *Nat. Commun.* **10**, 2253 (2019).
76. Panday, A. et al. FANCM regulates repair pathway choice at stalled replication forks. *Mol. Cell* **81**, 2428–2444 e6 (2021).
77. Morawska, M. & Ulrich, H. D. An expanded tool kit for the auxin-inducible degron system in budding yeast. *Yeast* **30**, 341–351 (2013).
78. Wach, A. PCR-synthesis of marker cassettes with long flanking homology regions for gene disruptions in *S. cerevisiae*. *Yeast* **12**, 259–265 (1996).
79. Goldstein, A. L. & McCusker, J. H. Three new dominant drug resistance cassettes for gene disruption in *Saccharomyces cerevisiae*. *Yeast* **15**, 1541–1553 (1999).
80. Pham, N. et al. Mechanisms restraining break-induced replication at two-ended DNA double-strand breaks. *EMBO J.* **40**, e104847 (2021).
81. Elango, R., Kockler, Z., Liu, L. & Malkova, A. Investigation of Break-Induced Replication in Yeast. *Methods Enzymol.* **601**, 161–203 (2018).
82. Garcia, P. D. et al. Stability and nuclear localization of yeast telomerase depend on protein components of RNase P/MRP. *Nat. Commun.* **11**, 2173 (2020).
83. Meza, E., Munoz-Arellano, A. J., Johansson, M., Chen, X. & Petranovic, D. Development of a method for heat shock stress assessment in yeast based on transcription of specific genes. *Yeast* **38**, 549–565 (2021).
84. Holmes, A. & Haber, J. E. Physical monitoring of HO-induced homologous recombination. *Methods Mol. Biol.* **113**, 403–415 (1999).
85. Sneath, P. H. & Sokal, R. R. Numerical taxonomy. *Nature* **193**, 855–860 (1962).
86. Tamura, K., Stecher, G. & Kumar, S. MEGA11: Molecular Evolutionary Genetics Analysis Version 11. *Mol. Biol. Evol.* **38**, 3022–3027 (2021).
87. Kimura, M. A simple method for estimating evolutionary rates of base substitutions through comparative studies of nucleotide sequences. *J. Mol. Evol.* **16**, 111–120 (1980).
88. Mouakkad-Montoya, L. *et al*. Quantitative assessment reveals the dominance of duplicated sequences in germline-derived extrachromosomal circular DNA. *Proc Natl Acad Sci USA* **118** (2021).
89. Green, M. R. & Sambrook, J. Southern Blotting. *Cold Spring Harb Protoc* **2021** (2021).
90. Wells, J. M., Highly mutagenic copying of telomeric circles promotes ALT establishment, TeloTracker, https://doi.org/10.5281/zenodo.18918914 (2026).
91. Comeron, J. M., Highly mutagenic copying of telomeric circles promotes ALT establishment, Yeast-Telomere-Dynamics, https://doi.org/10.5281/zenodo.18751885 (2026).

Acknowledgements

We thank Dr. James E. Haber and the members of the Malkova Lab for insightful discussions and comments on this manuscript. This work was supported by NIA grant R01AG081263 to A.M. and J.M.C, by NIGMS grant R35GM127006 to AM, and by RR240030 grant from CPRIT to A.M.

Author contributions

M-C.T., J.M.W., Anna Malkova, and J.M.C. designed the study. M-C.T., K.A.R., and K.M. performed genetic and molecular biological experiments. J.M.W., J.M.C., and R.P. developed bioinformatic pipelines. J.M.W., A.Malkov, and J.M.C. performed bioinformatic analysis. J.M.C. performed computational modeling. M-C.T., J.M.W., K.A.R., K.M., Anna Malkova, and J.M.C. analyzed the data. M-C.T., J.M.W., K.A.R., Anna Malkova, and J.M.C. wrote the manuscript.

Competing interests

The authors declare no competing interests.

Additional information

Supplementary information The online version contains supplementary material available at https://doi.org/10.1038/s41467-026-72032-4.

Correspondence and requests for materials should be addressed to Josep M. Comeron or Anna Malkova.

Peer review information *Nature Communications* thanks the anonymous reviewer(s) for their contribution to the peer review of this work. A peer review file is available.